Electronic Supporting Information

Selective B–B Bond Activation in an Unsymmetrical Diborane(4) by $[(Me_3P)_4Rh–X]$ (X = Me, O*t*Bu): A Switch of Mechanism?

Corinna Borner, Kai Brandhorst and Christian Kleeberg*

Institut für Anorganische und Analytische Chemie,
Technische Universität Carolo-Wilhelmina zu Braunschweig,
Hagenring 30, 38106 Braunschweig, Germany.

* Author E-mail Address: ch.kleeberg@tu-braunschweig.de

Contents

1. Experimental Data and Additional Results

a. General Considerations

[$(Me_3P)_4Rh$]Cl, [$(Me_3P)_4RhMe$] (**1a**), pinB–Bdmab (**2a**), pinB–Bdbab (**2b**) and [(18-C-6)K][dmabB–B(O*t*Bu)pin] were prepared following literature procedures.[S1,S2] All other compounds were commercially available and used as received. Benzene was dried over potassium/benzophenone and degassed before use. All other solvents were dried using MBraun solvent purification systems, deoxygenated using the freeze-pump-thaw method and stored under purified nitrogen. All manipulations were performed using standard Schlenk techniques under an atmosphere of purified nitrogen or in a nitrogen filled glove box (MBraun). NMR spectra were recorded using Bruker Avance II 300, Bruker Avance 400, Bruker DRX 400 or Bruker Avance II 600 spectrometers. Air sensitive samples were measured in NMR tubes equipped with screw caps (Wilmad) or flame-sealed NMR tubes. Chemical shifts (δ) are given in ppm, using the residual resonance signal of the solvents as internal reference (C_6D_6: ^{1}H NMR: 7.16 ppm, ^{13}C NMR: 128.06 ppm; THF-d_8: ^{1}H NMR: 1.72 ppm, ^{13}C NMR: 25.31 ppm).[S3] ^{11}B and ^{31}P chemical shifts are reported relative to external $BF_3 \cdot Et_2O$ and 85% H_3PO_4, respectively. C_6D_6 and THF-d_8 (Eurisotop, 99.5% deuteration) were dried over potassium/ benzophenone and degassed before use. ^{11}B NMR spectra were generally processed applying a Lorentz type window function (LB = 10 Hz) and using a back linear prediction in order to suppress the broad background signal due to the borosilicate glass of the NMR tube; the spectra were carefully evaluated to ensure that no genuinely broad signals of the sample were suppressed. $\Delta w_{½}$ refers to the full signal width at half-height. If necessary, coupling patterns were analysed with the aid of simulations (DAISY/TOPSPIN). For measurements of ^{11}B, ^{31}P and ^{13}C nuclei broadband composite pulse ^{1}H decoupling was applied unless stated otherwise. Melting points were determined using a Büchi 530 apparatus in flame sealed capillaries under nitrogen and are not corrected. Elemental analyses were performed using an Elementar vario MICRO cube instrument at the Institut für Anorganische und Analytische Chemie of the Technische Universität Carolo-Wilhelmina zu Braunschweig. GC/MS measurements were performed using a Shimadzu GCMS-QP2010SE instrument operating in positive EI mode (70 eV, 60 –

700 m/z) using the following conditions: injection temperature 250 °C; interface temperature 280 °C; temperature program: start temperature 50 °C for 3 min, heating rate 12 °C min^{-1}, end temperature 300 °C for 8 min; column type: ZB-5MS GUARDIAN, 30 m × 0.25 mm, 0.25 μm film thickness; helium as carrier gas (1.5 mL min^{-1}). EI mass spectra were recorded using a Finnigan MAT 95 XP instrument at 70 eV. Note that the samples were prepared inside a nitrogen filled glovebox but had to be exposed briefly to air during the transfer into the instrument.

b. [(Me$_3$P)$_4$Rh-O*t*Bu] (1b)

NMR experiment: [(Me$_3$P)$_4$Rh]Cl (13.0 mg, 29 μmol, 1 eq) was placed in an screw-cap NMR tube and dry THF-d$_8$ (0.6 mL) was added. Upon addition of KO*t*Bu (3.3 mg, 29 μmol, 1 eq) the [(Me$_3$P)$_4$Rh]Cl dissolves and a bright orange-yellow solution was formed within a few minutes. VT-NMR spectra of the sample were recorded (Figure S1).

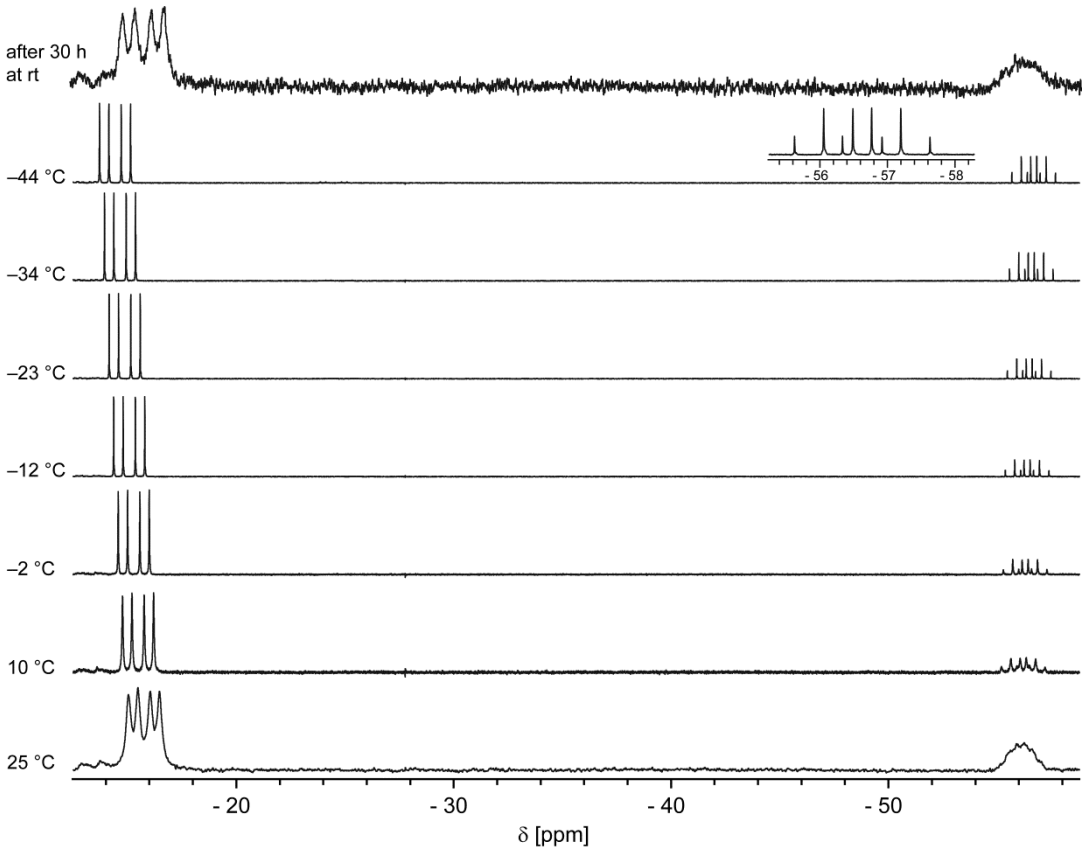

Figure S1. $^{31}P\{^1H\}$ VT-NMR spectra of an equimolar mixture of [(Me$_3$P)$_4$Rh]Cl and KO*t*Bu and a spectrum of this mixture after 30 h at rt (162/122 MHz, rt, THF-d$_8$).

Yield: According to the NMR data **1b** is formed virtually quantitatively (>95%). Within 30 h at ambient temperature only marginal decomposition is observed (Figure S1).

δ_H (400 MHz; THF-d$_8$, rt) 1.13 (9 H, br s, O*t*Bu), 1.23 (27 H, br s, Me$_3$P$_{eq}$), 1.37 (9 H, br dd, J = 9 Hz, J = 1 Hz, Me$_3$P$_{ax}$).

δ_P (162 MHz; THF-d$_8$, rt) –15.7 (3 P, br dd, $J_{P\text{-}Rh}$ = 160 Hz, $J_{P\text{-}P}$ = 69 Hz, Me$_3$P$_{eq}$, $\Delta w_{½}$ = 46 Hz), –56.1 (1 P, br s, Me$_3$P$_{ax}$, $\Delta w_{½}$ = 129 Hz).

δ_H (400 MHz; THF-d_8, 250 K) 1.12 (9 H, br s, O*t*Bu), 1.23 (27 H, br s, Me_3P_{eq}, $\Delta w_{½}$ = 6.5 Hz), 1.37 (9 H, d, $J_{P\text{-}P}$ = 8.7 Hz, Me_3P_{ax}).

δ_C (100 MHz; THF-d_8, 250 K) 18.8 (qd, J = 9.3 Hz, J = 2.9 Hz, Me_3P), 26.3 (m, Me_3P), 31.7 (s, $C(CH_3)_3$), quaternary $C(CH_3)_3$ signal not detected, due to overlapping with solvent signal.

δ_P (162 MHz; THF-d_8, 250 K) –14.8 (3 P, dd, $J_{P\text{-}Rh}$ = 162 Hz, $J_{P\text{-}P}$ = 70 Hz, Me_3P_{eq}, $\Delta w_{½}$ = 2.3 Hz), –56.4 (1 P, dq, $J_{P\text{-}Rh}$ = 114 Hz, $J_{P\text{–}P}$ = 70 Hz, Me_3P_{ax}, $\Delta w_{½}$ = 2 Hz).

Attempted isolation of ***1b****; formation of* $[(Me_3P)_2Rh\text{–}CH_2\text{–}PMe_2]_2$*:* $[(Me_3P)_4Rh]Cl$ (52 mg, 117 μmol, 1 eq) and KO*t*Bu (13 mg, 116 μmol, 1 eq) were mixed in dry THF (3 mL). After stirring for 2 h at ambient temperature virtually all of the $[(Me_3P)_4Rh]Cl$ had dissolved and the solution was filtered over Celite and layered with *n*-pentane (5 mL). Within a few days at –40 °C well-developed orange-red crystals of $[(Me_3P)_2Rh\text{–}CH_2\text{–}PMe_2]_2$ separated. In our hands all further attempts to isolate **1b** by using other solvents (mixtures), reaction times or conditions led consistently to the isolation of $[(Me_3P)_2Rh\text{–}CH_2\text{–}PMe_2]_2$.

$[(Me_3P)_2Rh\text{–}CH_2\text{–}PMe_2]_2$ has been reported in the literature but crystallographic and spectroscopic data are not readily accessible and hence are reported here again.[S4]

Yield: 21 mg, 32 μmol, 55%.

Found: C, 32.47; H, 7.98.
Calc. for $C_{18}H_{52}P_6Rh_2$: C, 32.74; H, 7.94%.

δ_H (400 MHz; C_6D_6; rt) 1.04 (4 H, br s, $(CH_2)PMe_2$, $\Delta w_{½}$ = 21 Hz), 1.23 (18 H, br d, PMe_3, J = 5.4 Hz, $\Delta w_{½}$ = 3.2 Hz), 1.26 (18 H, br d, PMe_3, J = 5.4 Hz, $\Delta w_{½}$ = 1.7 Hz), 1.69 (12 H, br d, $(CH_2)P(CH_3)_2$, J = 5.3 Hz, $\Delta w_{½}$ = 3.6 Hz).

δ_C (100 MHz; C_6D_6; rt) 10.7–11.9 (br m, $(CH_2)PMe_2$), 20.2 (d, J = 19 Hz, PMe_3), 23.5 (d, J = 18 Hz, PMe_3), 26.8 (d, J = 14 Hz, $(CH_2)P(CH_3)_2$).

δ_P (162 MHz; C_6D_6, rt) – 4.2 – (–8.2) (m), – 9.8 – (–11.7) (m), – 12.8 – (–14.1) (m). See also Figure S2.

mp: >110 °C decomp.; a black liquid is formed >130 °C.

m/z (EI$^+$) 584 ([M–PMe_3]$^+$, 1), 255 ([$C_6H_{18}P_2Rh$]$^+$, 6), 76 ([PMe_3]$^+$, 71), 61 ([C_2H_6P]$^+$, 100).

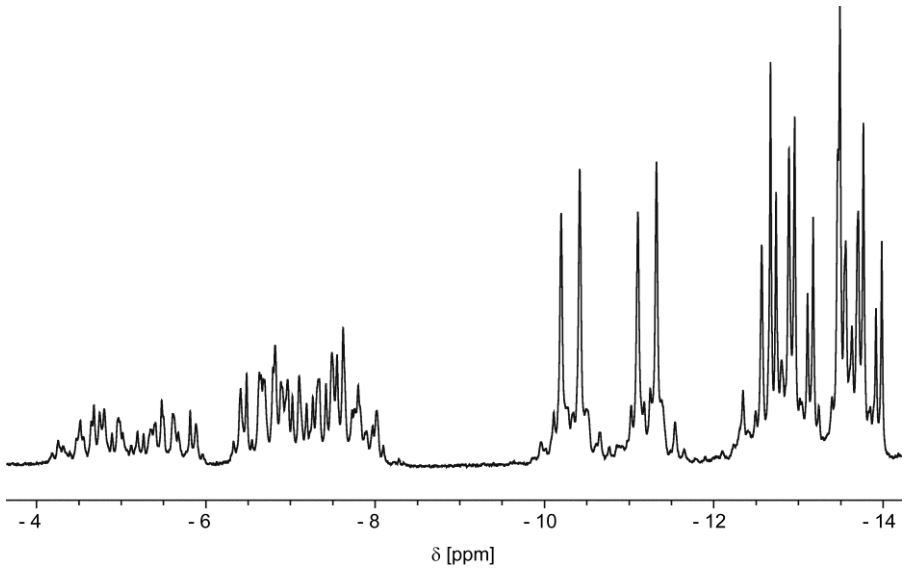

Figure S2. $^{31}P\{^1H\}$ NMR spectrum of [$(Me_3P)_2Rh–CH_2–PMe_2]_2$ (162 MHz, rt, C_6D_6).

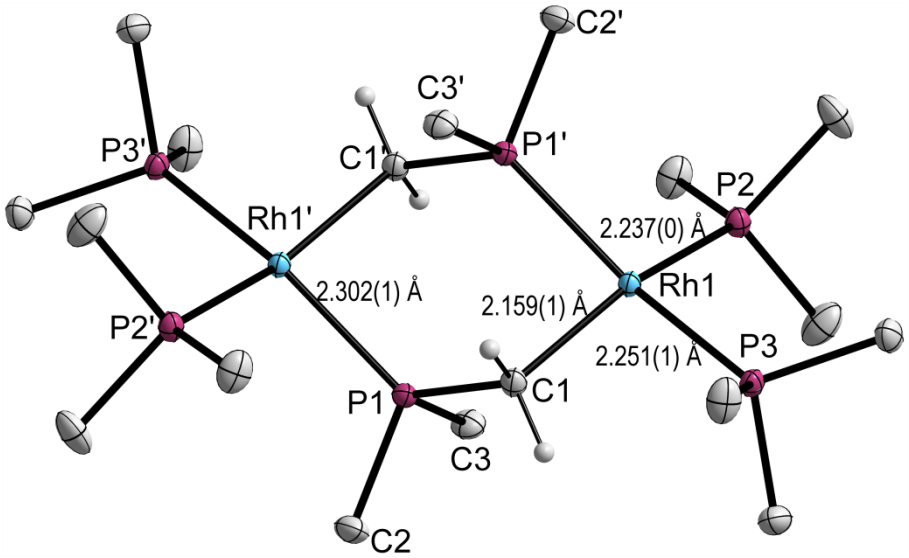

Figure S3. Molecular structure of [$(Me_3P)_2Rh–CH_2–PMe_2]_2$.

c. [$(Me_3P)_3$Rh-Bdmab] (4a)

$[(Me_3P)_4Rh]Cl$ (100 mg, 226 μmol, 1 eq) and pinB–Bdmab (**2a**) (61 mg, 226 μmol, 1 eq) were combined in dry THF (2 mL). After stirring for a few minutes at ambient temperature KO*t*Bu (25 mg, 226 μmol, 1 eq, dissolved in dry THF (1 mL)) was added. The orange reaction mixture was stirred overnight at ambient temperature. After removing all volatiles *in vacuo* the residue was extracted with *n*-pentane and filtered over Celite. Within six days at –40°C **4a** separated as orange crystals suitable for single crystal analysis.

Altering the order of addition of the starting materials did, according to *in situ* NMR experiments (see paragraph 1f), not influence the outcome of the reaction.

Yield: 46 mg, 97 μmol, 43%.

Found: C, 42.50; H, 7.98; N, 5.70.
Calc. for $C_{17}H_{37}N_2BP_3Rh$: C, 42.88; H, 7.83; N, 5.88%.

δ_H (300 MHz; C_6D_6; rt) 0.98–1.03 (18 H, br m, $J_{H\text{-}P}$ = 1.2 Hz, $Me_3P_{cis\text{-}B}$), 1.12 (9 H, br d, $J_{H\text{-}P}$ = 4.1 Hz, $\Delta w_{½}$ = 1.5 Hz, $Me_3P_{trans\text{-}B}$), 3.46 (6 H, s, NCH_3), 6.95–7.02 (2 H, m, CH_{Ar}), 7.11–7.18 (2 H, m, CH_{Ar}).

δ_C (75 MHz; C_6D_6; rt) 21.8–22.5 (m, PMe_3), 32.9 (NCH_3), 105.5 (CH_{Ar}), 117.0 (CH_{Ar}), 141.3 (C_{Ar}).

δ_P (122 MHz; C_6D_6; rt) –24.8 (1 P, br d, $J_{P\text{-}Rh}$ = 77 Hz, $\Delta w_{½}$ = 105 Hz, $Me_3P_{trans\text{-}B}$), –14.1 (2 P, br dd, $J_{P\text{-}Rh}$ = 150 Hz, $J_{P\text{-}P}$ = 32 Hz, $\Delta w_{½}$ = 8 Hz, $Me_3P_{cis\text{-}B}$).

δ_B (96 MHz; C_6D_6; rt) 52.2 (br s, $\Delta w_{½}$ = 368 Hz, Bdmab).

δ_H (400 MHz; THF-d_8; rt) 1.09–1.12 (18 H, br m, $Me_3P_{cis\text{-}B}$), 1.33 (9 H, br d, $J_{H\text{-}P}$ = 4.1 Hz, $\Delta w_{½}$ = 2.9 Hz, $Me_3P_{trans\text{-}B}$), 3.35 (6 H, s, NCH_3), 6.58–6.62 (4 H, m, CH_{Ar}).

δ_P (162 MHz; THF-d_8; rt) –24.7 (1 P, br s, $\Delta w_{½}$ = 194 Hz, $Me_3P_{trans\text{-}B}$), –14.1 (2 P, dd, $J_{P\text{-}Rh}$ = 150 Hz, $J_{P\text{-}P}$ = 32 Hz, $\Delta w_{½}$ = 7 Hz, $Me_3P_{cis\text{-}B}$).

δ_B (96 MHz; THF-d_8; rt) 52.7 (br s, $\Delta w_{½}$ = 344 Hz, Bdmab).

δ_H (400 MHz; THF-d_8; 188 K) 1.09 (18 H, br s, $\Delta w_{½}$ = 6.1 Hz, PMe_3), 1.32 (9 H, br d, $J_{H\text{-}P}$ = 4.3 Hz, $\Delta w_{½}$ = 2.8 Hz, PMe_3), 3.33 (6 H, s, $\Delta w_{½}$ = 2.7 Hz, NCH_3), 6.61 (4 H, br s, $\Delta w_{½}$ = 3.6 Hz, CH_{Ar}).

δ_P (162 MHz; THF-d_8; 188 K) –23.6 (1 P, dt, $J_{P\text{-}Rh}$ = 107 Hz, $J_{P\text{-}P}$ = 33 Hz, $\Delta w_{½}$ = 11 Hz, $Me_3P_{trans\text{-}B}$), –12.8 (2 P, dd, $J_{P\text{-}Rh}$ = 148 Hz, $J_{P\text{-}P}$ = 33 Hz, $\Delta w_{½}$ = 3 Hz, $Me_3P_{cis\text{-}B}$).

mp: >90 °C decomp.; a black liquid is formed >116 °C.

m/z (EI$^+$) 476 ([M]$^+$, 5), 400 ([M–PMe_3]$^+$, 10), 324 ([M–2PMe_3]$^+$, 10), 145 ([Bdmab]$^+$, 73), 76 ([PMe_3]$^+$, 76), 61 ([C_2H_6P]$^+$, 100).

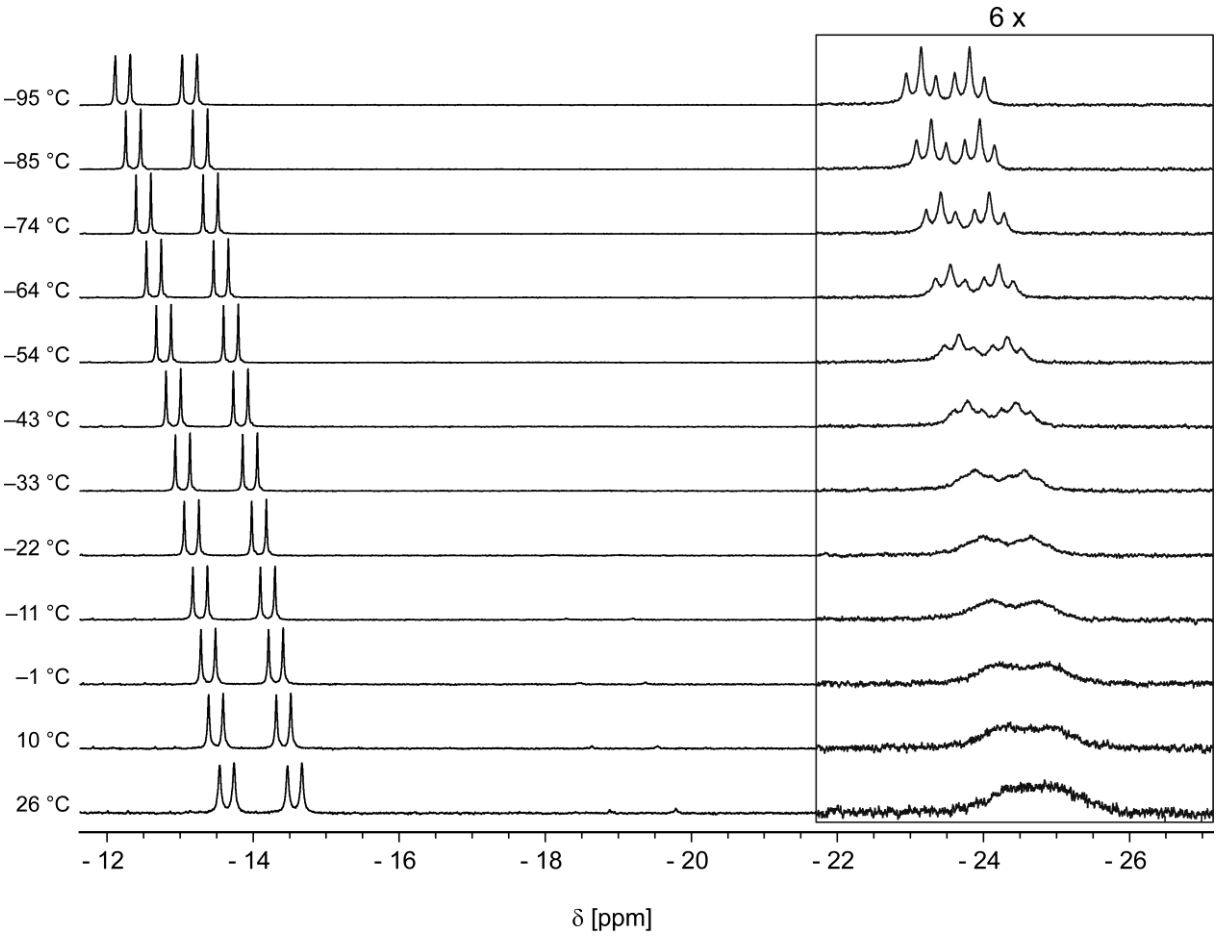

Figure S4. $^{31}P\{^1H\}$ VT-NMR spectra of **4a** (162 MHz, THF-d_8).

d. [$(Me_3P)_3$Rh-Bdbab] (4b)

[$(Me_3P)_4$Rh]Cl (48 mg, 113 μmol, 1 eq) and pinB–Bdbab (**2b**) (50 mg, 113 μmol, 1 eq) were combined in dry THF (1.5 mL). After stirring for a few minutes at ambient temperature KO*t*Bu (13 mg, 113 μmol, 1 eq, dissolved in dry THF (1 mL)) was added. The reaction mixture was stirred at ambient temperature overnight. After removing the volatiles *in vacuo* the residue was extracted with a mixture of *n*-pentane/toluene (approx. 2:1) and filtered over Celite. After a few days at –40°C **4b** separated as crystals suitable for single crystal analysis.

Yield: 11 mg, 17 μmol, 15%.

Found: C, 55.62; H, 7.51; N, 4.36.
Calc. for $C_{29}H_{45}N_2BP_3Rh$: C, 55.44; H, 7.22; N, 4.25%.

δ_H (600 MHz; THF-d_8; rt) 0.95–1.00 (18 H, br m, $Me_3P_{cis\text{-}B}$), 1.30 (9 H, d, J = 4.2 Hz, $Me_3P_{trans\text{-}B}$), 5.17 (4 H, s, NCH_2), 6.52–6.57 (2 H, m, CH_{dbab}), 6.58–6.63 (2 H, m, CH_{dbab}), 7.08–7.14 (2 H, m, $CH_{p\text{-}Ph}$), 7.16–7.21 (4 H, m, $CH_{m\text{-}Ph}$), 7.34–7.37 (4 H, m, $CH_{o\text{-}Ph}$).

δ_C (151 MHz; THF-d_8; rt) 21.7 (dt, J = 2.6 Hz, J = 12.8 Hz, $Me_3P_{trans\text{-}B}$), 22.2 (tdd, J = 2.6 Hz, J = 6.3 Hz, J = 12.6 Hz, $Me_3P_{cis\text{-}B}$), 51.5 (NCH_2), 107.6 ($CH_{o\text{-}dbab}$), 116.9 ($CH_{m\text{-}dbab}$), 126.7 ($CH_{p\text{-}Ph}$), 128.5 ($CH_{o\text{-}Ph}$), 128.6 ($CH_{m\text{-}Ph}$), 141.3 (d, J = 2.8 Hz, C_{dbab}), 142.8 (C_{Ph}).

δ_P (162 MHz; THF-d_8; rt) –24.6 (1 P, br d, $J_{P\text{-}Rh}$ = 94 Hz, $\Delta w_{½}$ = 93 Hz, $Me_3P_{trans\text{-}B}$), –14.8 (2 P, dd, $J_{P\text{-}Rh}$ = 149 Hz, $J_{P\text{-}P}$ = 33 Hz, $\Delta w_{½}$ = 5.3 Hz, $Me_3P_{cis\text{-}B}$).

δ_B (128 MHz; THF-d_8; rt) 55.1 (br s, $\Delta w_{½}$ = 550 Hz).

mp: 125–129 °C decomp.; a black residue is formed.

e. [(Me$_3$P)$_4$Rh–Bpin] (3)

[(Me$_3$P)$_4$Rh]Cl (100 mg, 226 μmol, 1 eq) and B_2pin_2 (57 mg, 226 μmol, 1 eq) were combined in dry THF (2 mL). After stirring for a few minutes at ambient temperature KO*t*Bu (25 mg, 226 μmol, 1 eq, dissolved in dry THF (1 mL)) was added. The orange reaction mixture was stirred at ambient temperature for 3.5 h. After removing the volatiles *in vacuo* the residue was extracted with *n*-pentane and filtered over Celite. Within five days at –40°C **3** separated as crystals suitable for single crystal analysis.

Yield: 29 mg, 54 μmol, 24%.

Found: C, 40.69; H, 9.39.
Calc. for $C_{18}H_{48}BO_2P_4Rh$: C, 40.47; H, 9.06%.

δ_H (300 MHz; C_6D_6; rt) 1.23 (12 H, s, $C_2(CH_3)_4$),
1.41 (36 H, br s, $\Delta w_{½}$ = 4.0 Hz, PMe_3).

δ_C (75 MHz; C_6D_6; rt) 26.9 ($C_2(CH_3)_4$), 27.3 (br s, $\Delta w_{½}$ = 4.0 Hz, PMe_3),
81.0 ($C_2(CH_3)_4$).

δ_P (122 MHz; C_6D_6; rt) –21.9 (d, $J_{P\text{-}Rh}$ = 144 Hz, $\Delta w_{½}$ = 40 Hz, PMe_3).

δ_B (96 MHz; C_6D_6; rt) 44.6 (br s, $\Delta w_{½}$ = 240 Hz, Bpin).

δ_H (300 MHz; THF-d_8; rt) 1.22 (12 H, s, $C_2(CH_3)_4$),
1.32 (36 H, br s, $\Delta w_{½}$ = 2.4 Hz, PMe_3).

δ_C (75 MHz; THF-d_8; rt) 27.1 ($C_2(CH_3)_4$), 27.2–27.6 (m, PMe_3), 81.5 ($C_2(CH_3)_4$).

δ_P (122 MHz; THF-d_8; rt) –21.8 (d, $J_{P\text{-}Rh}$ = 143 Hz, $\Delta w_{½}$ = 50 Hz, PMe_3).

δ_B (96 MHz; THF-d_8; rt) 45.0 (br s, $\Delta w_{½}$ = 180 Hz, Bpin).

δ_H (400 MHz; THF-d_8; 178 K) 1.21 (12 H, s, $\Delta w_{½}$ = 3.8 Hz, $C_2(CH_3)_4$),
1.31 (36 H, br s, $\Delta w_{½}$ = 7.2 Hz, PMe_3).

δ_P (162 MHz; THF-d_8; 178 K) –21.9 (3 P, dd, $J_{P\text{-}Rh}$ = 160 Hz, $J_{P\text{-}P}$ = 47 Hz,
$\Delta w_{½}$ = 3 Hz, Me_3P_{eq}), –12.9 (1 P, app sext.,
J = 46 Hz, $\Delta w_{½}$ = 21 Hz, Me_3P_{ax}).

mp: 79 – 81 °C.

m/z (EI$^+$) 458 ([M–PMe_3]$^+$, 2), 382 ([M–2PMe_3]$^+$, 3), 331 ([$(PMe_3)_3Rh$]$^+$, 3),
255 ([$(PMe_3)_2Rh$]$^+$, 10), 76 ([PMe_3]$^+$, 66), 61 ([C_2H_6P]$^+$, 100).

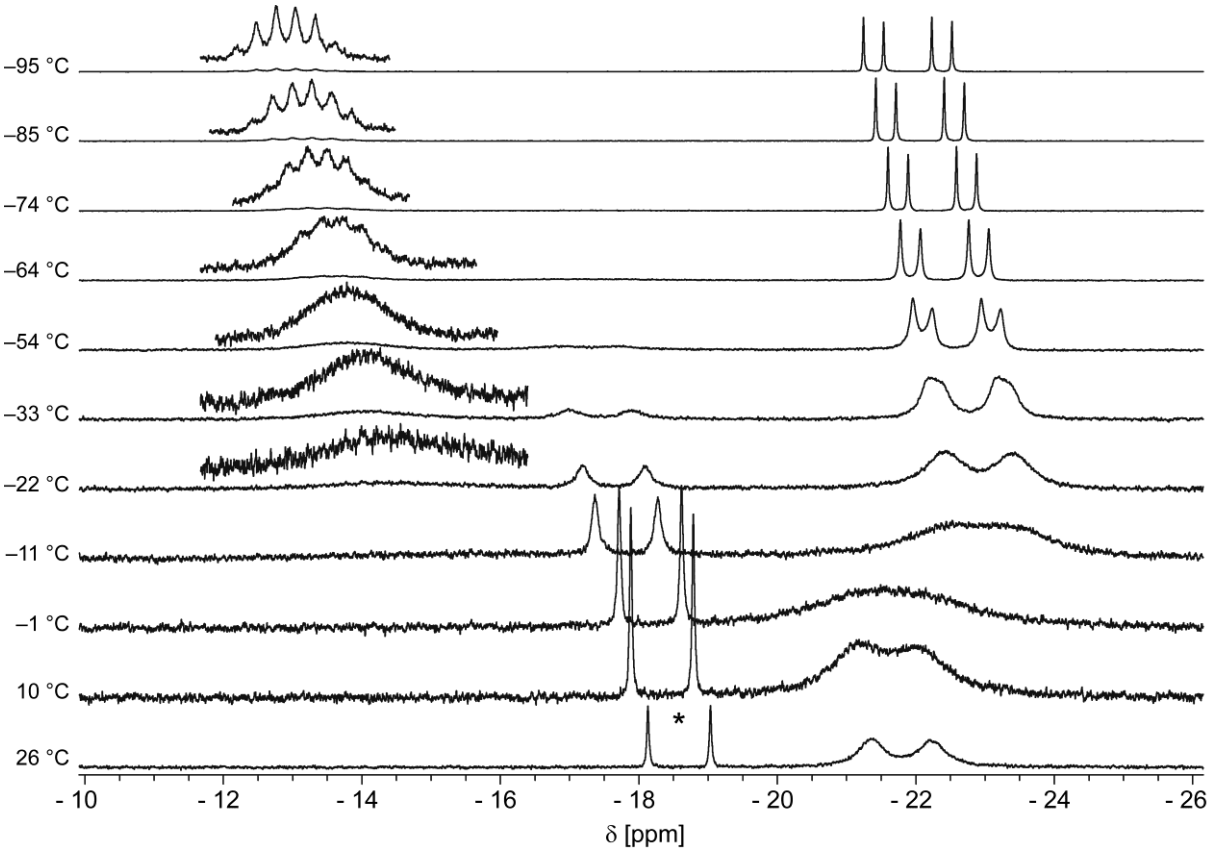

Figure S5. $^{31}P\{^{1}H\}$ VT-NMR spectra of **3** in THF-d_8;
* denotes an impurity of $[(Me_3P)_4Rh–H]$ (162 MHz).

The $^{11}B\{^{1}H\}$ NMR spectrum of **3** in THF-d_8 at ambient temperature exhibits a characteristic broad singlet at 45.0 ppm ($\Delta w_{½}$ = 180 Hz) whilst in the $^{31}P\{^{1}H\}$ NMR spectrum a characteristic broad doublet at –21.8 ppm (J_{RhP} = 143 Hz, $\Delta w_{½}$ = 50 Hz) is observed (Figure S5). The latter signal indicates fluxional behaviour in solution as it sharpens upon cooling to –95 °C to give an apparent sextet (in agreement with simulations of doublet of quartets with –12.9 ppm, $J_{P–P}$ = 47 Hz, $J_{P\text{-}Rh}$ = 95 Hz, $\Delta w_{½}$ = 22 Hz) and a doublet of doublets (–21.9 ppm, $J_{P\text{-}P}$ = 47 Hz, $J_{P\text{-}Rh}$ = 160 Hz, $\Delta w_{½}$ = 3 Hz) indicating a trigonal-bipyramidal structure (Figure S5).

These NMR data agree with those of the related complex $[(Me_3P)_4Rh–Bcat]$ (rt: ^{11}B 49.0 ppm (br s) ^{31}P: –21.9 ppm (dd, $J_{P\text{-}Rh}$ = 137 Hz); 193 K: ^{31}P: –22.0 ppm (dd, $J_{P\text{-}P}$ = 48 Hz, $J_{P\text{-}Rh}$ = 157 Hz, , 3 P), –13.2 ppm (dq, $J_{P\text{-}P}$ = 48 Hz, $J_{P\text{-}Rh}$ = 91 Hz, 1 P)).[S5a] In addition the $^{31}P\{^{1}H\}$ NMR spectra exhibit a doublet at –18.6 ppm indicative for $[(Me_3P)_4Rh–H]$ with an integral corresponding to 13% relative to **3**.[S6]

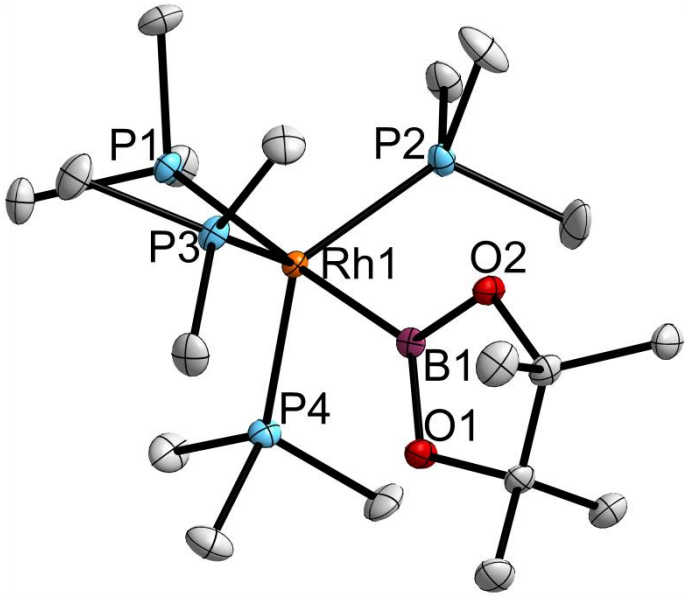

Figure S6 Molecular structure of **3**. Selected bond lengths and angles for **3** B1–Rh1 2.104(3) Å, P1–Rh1 2.3299(7) Å, P2–Rh1 2.3002(9) Å, P3–Rh1 2.2816(7) Å, P4–Rh1 2.2946(8) Å, B1–Rh1–P1 174.48(9)°, B1–Rh1–P2 84.1(1)°, B1–Rh1–P3 81.42(7)°, B1–Rh1–P4 86.3(1)°, P2–Rh1–P3 120.36(3)°, P3–Rh1–P4 115.98(3)°, P4–Rh1–P2 120.37(3)°, P1–Rh1–P2 94.46(3)°, P1–Rh1–P3 96.58(2)°, P1–Rh1–P4 97.15(3)°. For clarity hydrogen atoms are omitted; thermal ellipsoids are drawn at the 50% probability level.

In the solid state complex **3** exhibits a trigonal-bipyramidal structure with an axial boryl ligand (Figure S6). The geometrical parameters comparable with those of the analogous complex [$(Me_3P)_4$Rh–Bcat] (Rh–B 2.047(2) Å, Rh–P_{ax} 2.3404(6) Å, Rh–P_{eq} 2.3049(6) Å, 2.2891(6) Å, 2.3096(6) Å).[S5a] Noteworthy, a slightly shorter *trans*-boryl Rh–P distance for **3** suggests a weaker *trans*-influence of the Bpin ligand as of the Bcat ligand contradicting the trend established computationally for a series of boryl-Pt^{II} complexes.[S5b,c]

f. NMR spectroscopic study of the reaction of 2a with Rh(I) complexes

*i) Reaction of **2a** with **1a***

In a nitrogen filled glovebox a screw cap NMR tube was charged with [$(Me_3P)_4RhMe$] (10 mg, 24 μmol, 1 eq), **2a** (6 mg, 24 μmol, 1 eq) and C_6D_6 or THF-d_8 (0.7 mL) and NMR spectra were recorded.

*ii) Reaction of **2a** with **1b***

In a nitrogen filled glovebox a screw cap NMR tube was charged with [$(Me_3P)_4Rh$]Cl (13.0 mg, 29 μmol, 1.0 eq), KO*t*Bu (3.3 mg, 29 μmol, 1.0 eq) and THF-d_8 (0.7 mL). After 5 min virtually all of the materials dissolved to give a bright light orange solution of [$(Me_3P)_4Rh$–O*t*Bu] (see also under b.). After addition of **2a** (9 mg, 33 μmol, 1.1 eq) NMR spectra were recorded.

iii) Reaction of [(18-C-6)K][dmabB–B(OtBu)pin] with [$(Me_3P)_4Rh$]Cl

In a nitrogen filled glovebox a screw cap NMR tube was charged with [$(Me_3P)_4Rh$]Cl (5 mg, 11 μmol, 1 eq), [(18-C-6)K][dmabB–B(O*t*Bu)pin][S1] (7 mg, 11 μmol, 1 eq) and THF-d_8 (0.7 mL) and NMR spectra were recorded.

*iv) Reaction of [$(Me_3P)_2Rh–CH_2–PMe_2]_2$ with **2a***

In a nitrogen filled glovebox a screw cap NMR tube was charged with [$(Me_3P)_2Rh–CH_2–PMe_2]_2$ (16 mg, 24 μmol, 1 eq), **2a** (6 mg, 24 μmol, 1 eq) and THF-d_8 (0.7 mL) and NMR spectra were recorded.

• *Reaction of **2a** with **1a** in THF-d_8*

The *in situ* $^{11}B\{^1H\}$ and $^{31}P\{^1H\}$ NMR spectra of the reaction of **1a** with **2a** in THF-d_8 (Figure S7) indicate that both **3** and **4a** are formed accompanied with appreciable amounts of unidentified species. The relative amounts of **3** and **4a** may be estimated with due care (see below) to a ratio of 2:1 in favour of **4a**.

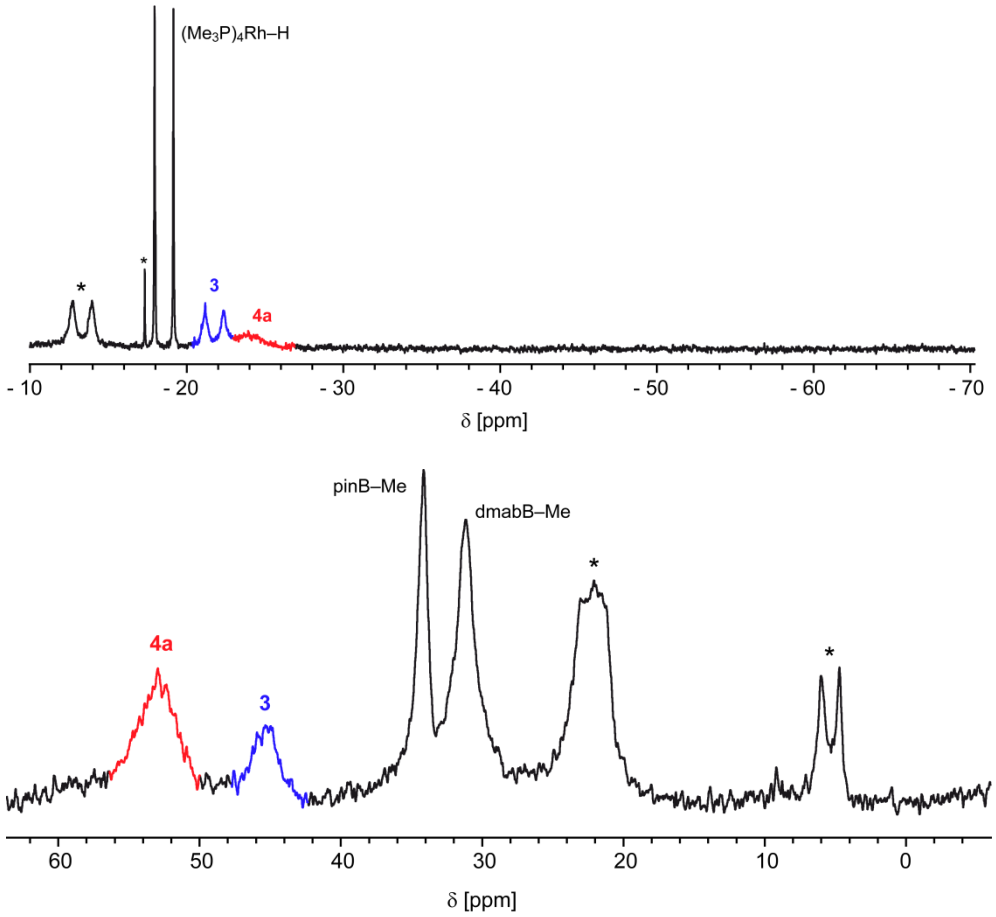

Figure S7. *In situ* $^{31}P\{^{1}H\}$ (top) and $^{11}B\{^{1}H\}$ NMR (bottom) spectra of the reaction of $[(Me_3P)_4RhMe]$ (**1a**) with **2a** in THF-d_8 after 16 h at rt (rt, 122 MHz/96 MHz, THF-d_8, * unidentified species, see also references 9a,b and 11).

• *Reaction of **2a** with **1b** – Influence of the order of Addition*

An NMR experiment analogous to that described in the main text but reversing the order of addition was performed (Figure S8, bottom). According to *in situ* ^{31}P and ^{11}B NMR spectroscopy B–B activation under predominant formation of **4a** takes place, as for the initial order of addition; the observed by-products also resemble those found for the initial order of addition. It should be noted that during this reaction no homogeneous solution was obtained; furthermore, the ^{31}P NMR signal of **4a** in exchange with PMe_3 is significantly broader and presumably overlapping.[S1] An additional experiment (not shown) showed that no reaction occurs under comparable conditions in the absence of KO*t*Bu.

Moreover, in a further experiment (Figure S8, top) the isolated adduct [(18-C-6)K][dmabB–B(O*t*Bu)pin] was reacted with an equimolar amount of $[(Me_3P)_4Rh]Cl$ (Figure S8, top).[S1] Whilst only marginal conversion was observed after 16 h at ambient temperature (not shown) more effective conversion – also slow and

accompanied by substantial formation of $[(Me_3P)_4RhH]$ – was observed after heating (4 h at 50 °C). This may be rationalised by the low solubility of $[(Me_3P)_4Rh]Cl$ in THF. However, importantly **4a** is again identified as the main product by ^{31}P and ^{11}B NMR spectroscopy.

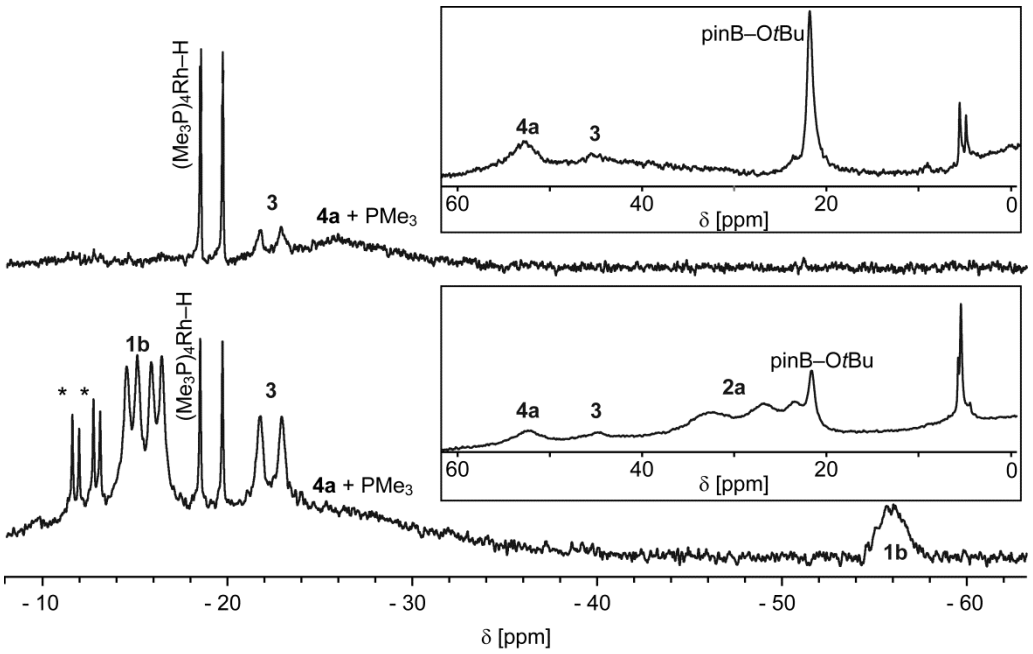

Figure S8. *In situ* $^{31}P\{^1H\}$ and $^{11}B\{^1H\}$ NMR (insets) spectra of the B–B activation of **2a**. *bottom*: combining first $[(Me_3P)_4Rh]Cl$ and **2a** and then adding KO*t*Bu (after 16 h at rt); *top*: reaction of equimolar amounts of $[(Me_3P)_4Rh]Cl$ and the isolated adduct [(18-C-6)K][dmabB–B(O*t*Bu)pin] (after 4 h at 50 °C); (rt, 122 MHz/96 MHz, THF-d_8)[S1]

• *Reaction of $[(Me_3P)_2Rh–CH_2–PMe_2]_2$ with **2a***

$[(Me_3P)_2Rh–CH_2–PMe_2]_2$, the decomposition product of **1b**, was also reacted with **2a**. NMR spectra recorded after 30 h at ambient temperature shows only a very small amount of B–B activation products besides some unidentified side-products (Figure S9). Whilst both boryl complexes **3** and **4a** are identified by their characteristic ^{11}B NMR signals the ^{31}P NMR signal of **4a** was not readily identified. As a consequence the relative amounts could not be estimated but the B–B activation appears to proceed slightly in favour of **4a**. Furthermore, it should be noted that the proposed concomitantly formed products of the B–B activation pinB–CH_2–PMe_2 and dmabB–CH_2–PMe_2 were neither identified by NMR spectroscopy nor by GC/MS analysis of the reaction mixture.

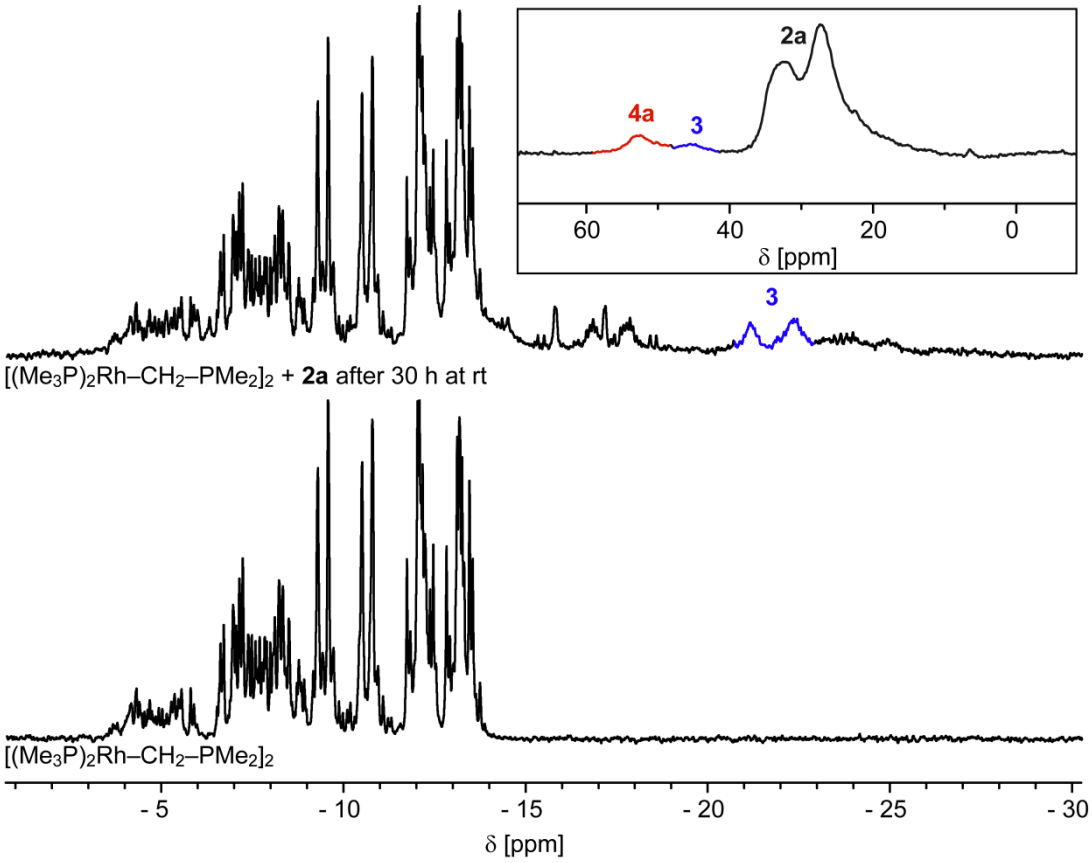

Figure S9. *In situ* $^{31}P\{^{1}H\}$ and $^{11}B\{^{1}H\}$ NMR (inset) spectra of the B–B activation of **2a** by $[(Me_3P)_2Rh–CH_2–PMe_2]_2$. (rt, 122 MHz/96 MHz, THF-d_8)

*Considerations on the selectivity of the B–B bond activation of **2a***

Determination of the relative amounts of **3** and **4a** formed by NMR spectroscopy is not straightforward. This is due to the very different relaxation behaviour, the dynamic processes present and the partly extensive peak overlap as well as the different NMR active nuclei present. In order to provide a rough estimation of the relative amounts individual values were determined by $^{31}P\{^{1}H\}$, $^{11}B\{^{1}H\}$ and ^{1}H NMR spectroscopy as well as by GC/MS analysis of the reaction mixtures (Table S1).

2a + 1a

	4a	**3**	pinB–Me	dmabB–Me
$^{31}P\{^{1}H\}$ NMR	0	100		
$^{11}B\{^{1}H\}$ NMR	<5	100	13	113
^{1}H NMR	16	100		
GC/MS			3	100

2a + 1b

	4a	**3**	pinB–O*t*Bu	dmabB–O*t*Bu
$^{31}P\{^{1}H\}$ NMR	100	7		
$^{11}B\{^{1}H\}$ NMR	100	4	104	Not unambiguously detected
^{1}H NMR	100	13		
GC/MS			100	4

Table S1. Relative amounts of **4a/3** and pinBX/dmabBX (X = Me, O*t*Bu) formed during the reaction of **2a**+**1a** and **2a**+**1b** as estimated by different methods.

Taking the values for the [**3**]:[**4a**] ratio obtained by different methods into account and also considering those of pinBX and dmabX (as the products formed concomitantly during the B–B bond activation) it may be stated that a selectivity of approximately 1:10 is obtained for the B–B bond activation by **1a** and **1b**, respectively, albeit with inverted selectivity.

g. *In situ* NMR spectroscopic study of the reaction of B_2pin_2 with 1b

Experimental Procedure

As described under f.ii), but using B_2pin_2 (8.4 mg, 33 μmol, 1.1 eq) instead of **2a**.

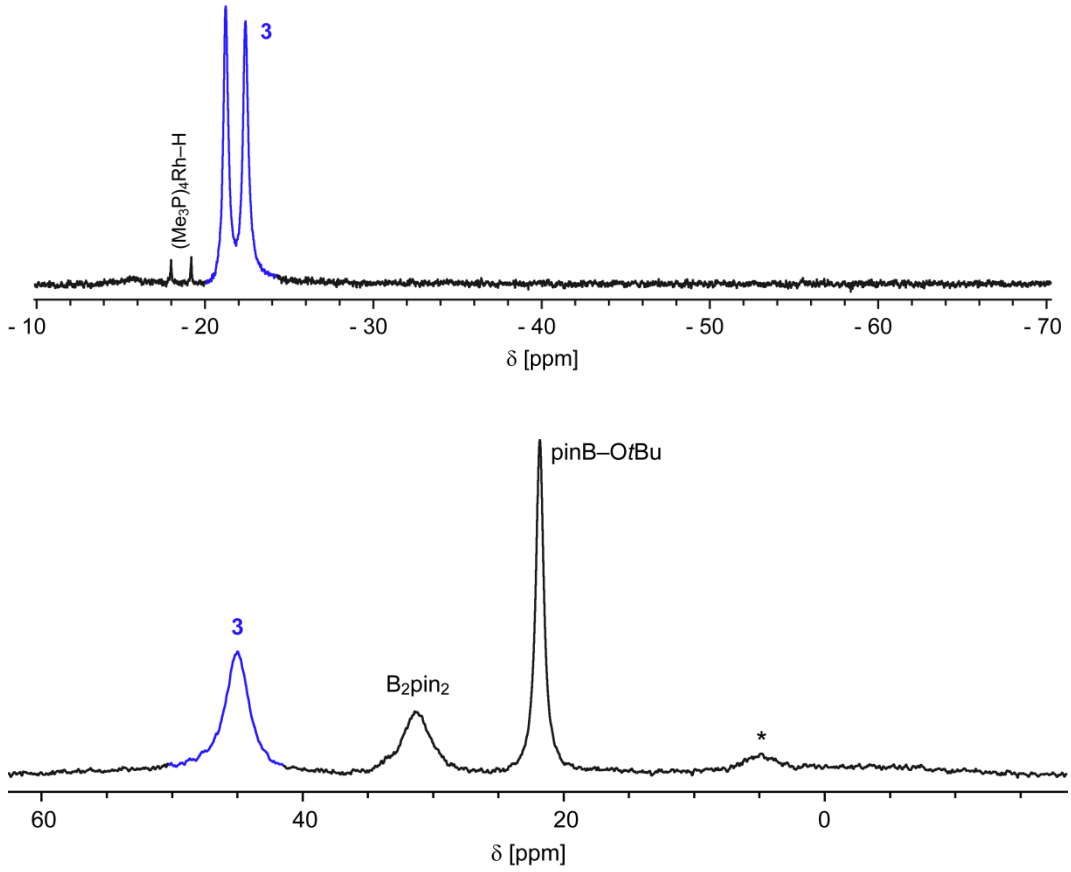

Figure S10. *In situ* $^{31}P\{^1H\}$ (top) and $^{11}B\{^1H\}$ NMR (bottom) spectra of the reaction of B_2pin_2 with **1b** after 7 h at rt (rt, 122 MHz/96 MHz, THF-d_8, * unidentified species (see also references 9c-e and 11)).

Results and Discussion

Monitoring the reaction of **1b** with B_2pin_2 at ambient temperature in THF-d_8 by *in situ* $^{31}P\{^1H\}$ and $^{11}B\{^1H\}$ NMR spectroscopy shows clearly that efficient conversion to the boryl complex **3** with only little by-product formation takes place (Figure S10).

h. Reaction of 4a with PMe_3 – $[(Me_3P)_4Rh–Bdmab]$ (5)

Experimental Procedure

In a nitrogen filled glovebox **4a** (10 mg, 21 μmol, 1 eq) was dissolved in C_6D_6 or THF-d_8 (0.7 mL) in a screw-cap NMR tube. To the deep orange solution different amounts of PMe_3 were added by means of a gas-tight microliter syringe (nominal amounts 0.5 eq, 1.5 eq, 20 eq, 15 – 20 eq and 10 eq, respectively). Upon addition of >1.5 eq PMe_3 the solution turned immediately yellow. ^{1}H, $^{31}P\{^{1}H\}$ and $^{11}B\{^{1}H\}$ NMR spectra were recorded.

Attempts to isolate **5** from mixtures containing **4a** and excess PMe_3 by crystallisation from THF and/or *n*-pentane solutions at –40 °C furnished repeatedly a yellow (according to optical inspection) crystalline material. This material turned reddish upon removal from the mother liquor and NMR analysis of the dried material were indicative for **4a**.

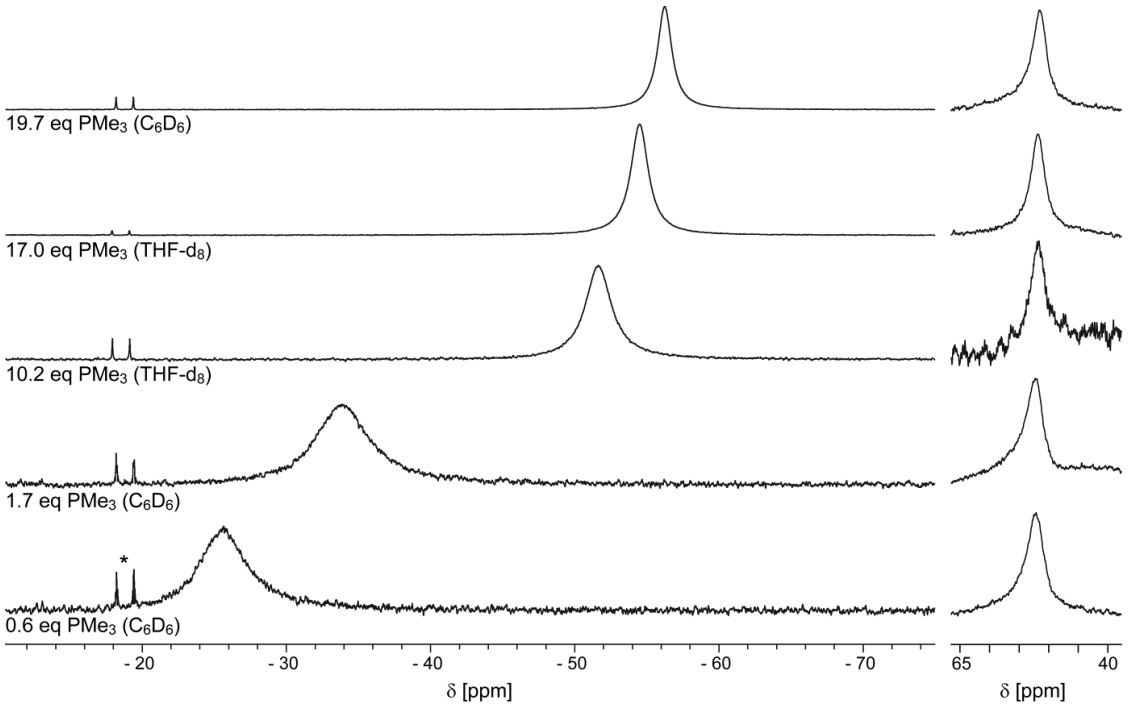

Figure S11. $^{31}P\{^{1}H\}$ (left) and $^{11}B\{^{1}H\}$ (right) spectra of **4a** in the presence of excess PMe_3; * denotes an impurity of $[(Me_3P)_4Rh–H]$ (all spectra at rt, 122 MHz/96 MHz).

The observed ^{31}P NMR chemical shift δ_P of mixtures of **4a** and PMe_3 in rapid exchange, putatively forming **5** in an equilibrium, are described by the weighted

average of the individual chemical shifts of free PMe_3 (δ_{PMe3}), **4a** (δ_{P3Rh}) and **5** (δ_{P4Rh}), respectively (the two latter being the weighted average of the chemical shifts of the different PMe_3 ligands). The parameters n_{Rh} and n_P refer to the relative overall amounts of (mononuclear) Rh-complexes and the overall amount of PMe_3 (free and bound). The parameters n_{PMe3}, n_{P3} and n_{P4} refer to the amount of free PMe_3, PMe_3 bound in **4a** and in **5**, n_{P3Rh} and n_{P4Rh} refer to the amount of **4a** and **5**, respectively. In addition the following relations are assumed:

(1) $n_{P3} = 3n_{P3Rh}$

(2) $n_{P4} = 4n_{P4Rh}$

(3) $n_P = n_{PMe_3} + n_{P3} + n_{P4} = n_{PMe_3} + 3n_{P3Rh} + 4n_{P4Rh}$

(4) $n_{Rh} = n_{P3Rh} + n_{P4Rh} = \frac{1}{3}n_{P3} + \frac{1}{4}n_{P4}$

$\delta_P = \frac{n_{P3}}{n_P}\delta_{P3Rh} + \frac{n_{P4}}{n_P}\delta_{P4Rh} + \frac{n_{PMe3}}{n_P}\delta_{PMe3}$

$= 3\frac{n_{P3Rh}}{n_P}\delta_{P3Rh} + 4\frac{n_{P4Rh}}{n_P}\delta_{P4Rh} + \frac{n_{PMe3}}{n_P}\delta_{PMe3}$ using (1) and (2)

$= 3\frac{n_{P3Rh}}{n_P}\delta_{P3Rh} + 4\frac{n_{P4Rh}}{n_P}\delta_{P4Rh} + \frac{(n_P - 3n_{P3Rh} - 4n_{P4Rh})}{n_P}\delta_{PMe3}$ using (3)

$= 3\frac{n_{P3Rh}}{n_P}\delta_{P3Rh} + 4\frac{n_{P4Rh}}{n_P}\delta_{P4Rh} - 3\frac{n_{P3Rh}}{n_P}\delta_{PMe3} - 4\frac{n_{P4Rh}}{n_P}\delta_{PMe3} + \delta_{PMe3}$

$= 3\frac{n_{P3Rh}}{n_P}(\delta_{P3Rh} - \delta_{PMe3}) + 4\frac{n_{P4Rh}}{n_P}(\delta_{P4Rh} - \delta_{PMe3}) + \delta_{PMe3}$

$= [3\, n_{P3Rh}(\delta_{P3Rh} - \delta_{PMe3}) + 4\, n_{P4Rh}(\delta_{P4Rh} - \delta_{PMe3})]\frac{1}{n_P} + \delta_{PMe3}$

$= [3\, n_{P3Rh}\delta_{P3Rh} - 3\, n_{P3Rh}\delta_{PMe3} + 4\, n_{P4Rh}\delta_{P4Rh} - 4\, n_{P4Rh}\delta_{PMe3}]\frac{1}{n_P} + \delta_{PMe3}$

$= [3\, n_{Rh}\delta_{P3Rh} - 3\, n_{P4Rh}\delta_{P3Rh} - 3\, n_{Rh}\delta_{PMe3} + 3\, n_{P4Rh}\delta_{PMe3} + 4\, n_{P4Rh}\delta_{P4Rh} - 4\, n_{P4Rh}\delta_{PMe3}]\frac{1}{n_P} + \delta_{PMe3}$ using (4)

$= [3\, n_{Rh}\delta_{P3Rh} - 3\, n_{P4Rh}\delta_{P3Rh} - 3\, n_{Rh}\delta_{PMe3} - n_{P4Rh}\delta_{PMe3} + 4\, n_{P4Rh}\delta_{P4Rh}]\frac{1}{n_P} + \delta_{PMe3}$

$= [3\, n_{Rh}(\delta_{P3Rh} - \delta_{PMe3}) - n_{P4Rh}(3\delta_{P3Rh} + \delta_{PMe3} - 4\,\delta_{P4Rh})]\frac{1}{n_P} + \delta_{PMe3}$

(6) $\delta_P = \left[3(\delta_{P3Rh} - \delta_{PMe3}) - (3\delta_{P3Rh} + \delta_{PMe3} - 4\,\delta_{P4Rh})\frac{n_{P4Rh}}{n_{Rh}}\right]\frac{n_{Rh}}{n_P} + \delta_{PMe3}$

In the final equation (6) only experimental accessible parameters, the chemical shifts δ_{P3Rh}, δ_{P4Rh} and δ_{PMe3} and the ratio $\frac{n_{Rh}}{n_P}$ are present, as well as the term $\frac{n_{P4Rh}}{n_{Rh}}$. As a consequence plotting the experimental determined ^{31}P NMR chemical shift against $\frac{n_{Rh}}{n_P}$ should result in a linear relation with an axis intercept of δ_{PMe3} and slope of

$$m = 3(\delta_{P3Rh} - \delta_{PMe3}) - (3\delta_{P3Rh} + \delta_{PMe3} - 4\,\delta_{P4Rh})\frac{n_{P4Rh}}{n_{Rh}}.$$

$\frac{n_{Rh}}{n_P}$ was determined by integration of the ^{1}H NMR spectra (NMe and PMe signals) and is in good agreement with the nominally added amount of PMe_3 (*vide supra*, Figure S11).

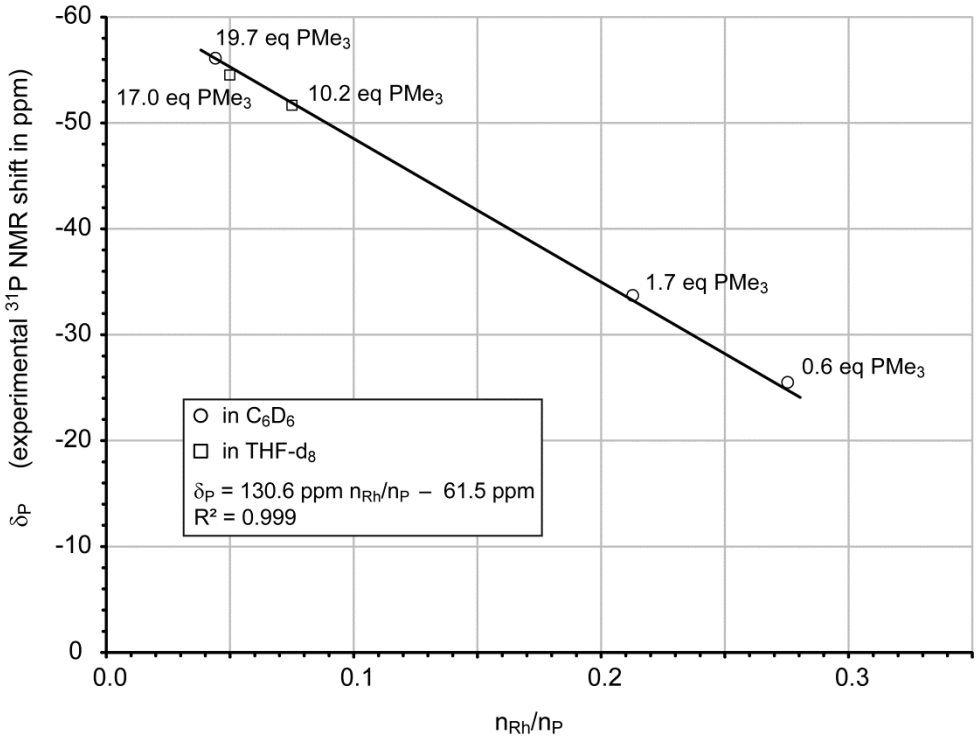

Figure S12. Plot of the measured ^{31}P NMR chemical shift of mixtures of **4a** and PMe_3 against $\frac{n_{Rh}}{n_P}$.

The term $\frac{n_{P4Rh}}{n_{Rh}}$ can now be determined from the fit function of the experimental data (Figure S12): from the slope of 130.6 ppm as well as the chemical shifts δ_{P3Rh}, δ_{PMe3}

and δ_{P4Rh} (the first two in C_6D_6 at rt, the latter at –96 °C in THF-d_8 assuming negligible solvent effects and temperature influence) follows

$$130.6 = 3(\delta_{P3Rh} - \delta_{PMe3}) - (3\delta_{P3Rh} + \delta_{PMe3} - 4\,\delta_{P4Rh})\frac{n_{P4Rh}}{n_{Rh}}$$

$$= 3(-17.7 + 62.0\,) - (-3 \cdot 17.7 - 62.0 + 4 \cdot 22.2)\frac{n_{P4Rh}}{n_{P3Rh} + n_{P4Rh}} = 132.9 - 26.3\frac{n_{P4Rh}}{n_{Rh}}$$

and finally $\frac{n_{P4Rh}}{n_{Rh}} = \frac{130.6-132.9}{-26.3} = 0.09$.

This value indicates that the equilibrium amount of **5** present in mixtures of **4a** and PMe_3 at rt is small. Hence, the observed ^{31}P NMR shift can be described reasonably well as only dependent on **4a** and PMe_3. The shift of the average ^{31}P NMR signal in fast exchange is described by the equation (following a similar reasoning as given for equation (6)):

(7) $$\delta_P = 3(\delta_{P3Rh} - \delta_{PMe3}) \cdot \frac{n_{Rh}}{n_P} + \delta_{PMe3}$$

Indeed, by using this equation the experimental values are quite well described. The fit function given in Figure S12 gives $\delta_{RhP3} - \delta_{PMe3}$ = 43.5 ppm and δ_{PMe3} = –61.5 ppm in good agreement with the expected values of $\delta_{RhP3} - \delta_{PMe3}$ = 44.3 ppm and δ_{PMe3} = –62.0 ppm calculated from the individual chemical shifts of **4a** and PMe_3 in C_6D_6.

However, the numbers obtained should be treated with some caution, as for δ_{P4Rh} the chemical shifts at –96 °C in THF-d_8 had to be used and a possible solvent and temperature dependence of the chemical shift has been assumed to be negligible. Nevertheless, in conclusion it may be stated that at ambient temperature, under the conditions studied, predominantly **4a** and free PMe_3 are in rapid exchange and that **5** is not present to more than 10 mol-%.

Note also, that for 1 eq excess of PMe_3 an average chemical shift of –28.9 ppm is calculated using equation (7) and the fitted parameters. This value agrees well with the signal at –27.4 ppm that was observed during the reaction of **2a** with **1b** (Figure 1).

A low temperature NMR study of a mixture of **4a** and 10.2 eq PMe_3 in THF-d_8, prepared as described above, was conducted (Figure S13, for discussion see main text (Figure 3)).

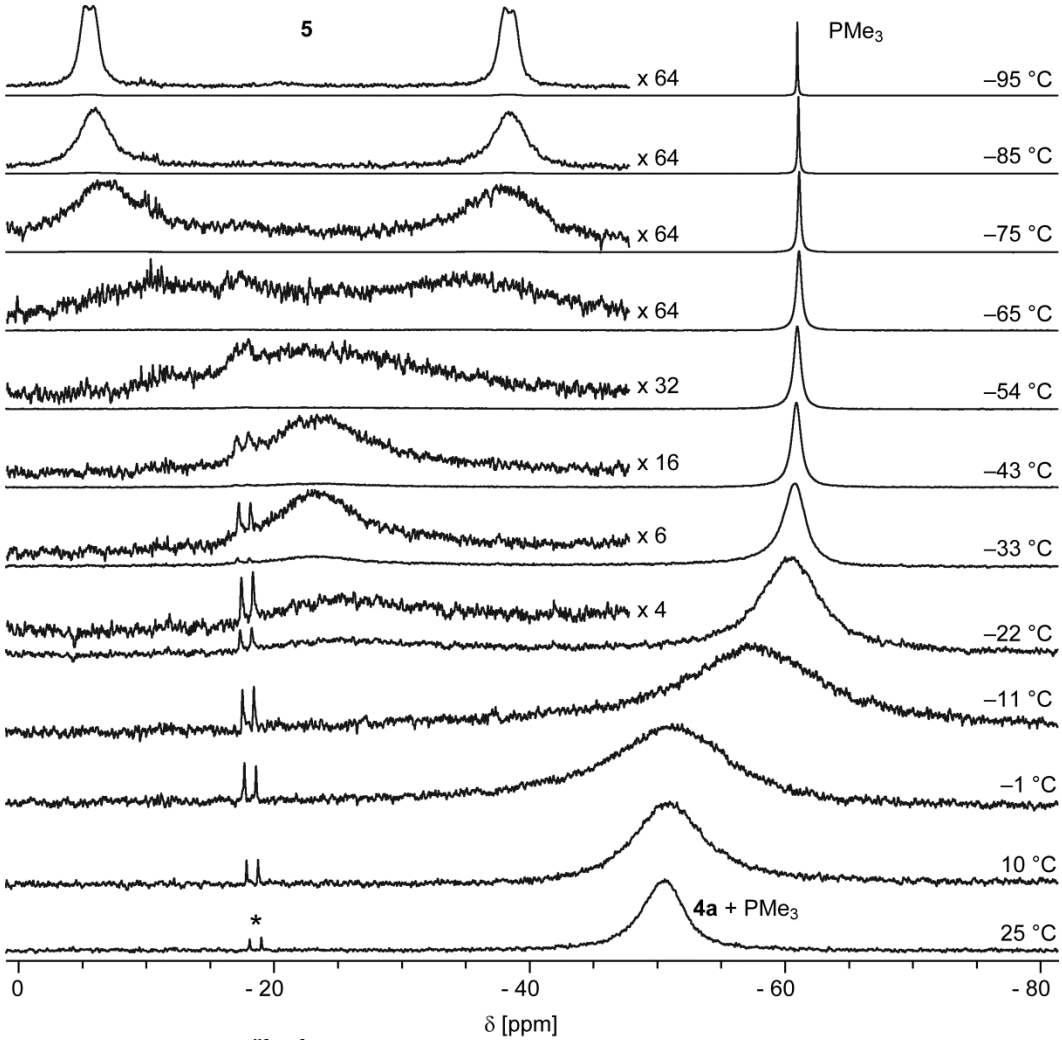

Figure S13. $^{31}P\{^1H\}$ VT-NMR spectra of **4a** in the presence of 10.2 eq of PMe_3 (THF-d_8, 162 MHz, * denotes an impurity of $[(Me_3P)_4Rh–H]$).

The following NMR data were obtained (in addition the signal of PMe_3 was detected (–95 °C, THF-d_8: ^1H NMR: 0.95 (br d, $J_{H\text{-}P}$ = 2 Hz, $\Delta w_{½}$ = 2.4 Hz, PMe_3), $^{31}P\{^1H\}$ NMR: –61.1 (br s, $\Delta w_{½}$ = 14.1 Hz, PMe_3)).

δ_H (400 MHz; THF-d_8; 178 K)	1.32 (36 H, br s, $\Delta w_{½}$ = 72 Hz, PMe_3), 3.56 (6 H, br s, $\Delta w_{½}$ = 3.6 Hz, NMe), 6.62–6.73 (4 H, m, CH_{Ar}).
δ_P (162 MHz; THF-d_8; 178 K)	–5.9 (2 P, $\Delta w_{½}$ = 400 Hz, PMe_3), –38.4 (2 P, $\Delta w_{½}$ = 430 Hz, PMe_3). The signal shape is suggestive for a pair of doublets ($J \approx 95$ Hz), though, not fully resolved.

i. Reaction of 4a with C_6H_6 and C_6D_6

Reaction with C_6H_6: In a nitrogen filled glovebox a screw cap NMR tube was charged with **4a** (5 mg, 11 μmol, 1 eq) dissolved in THF-d_8 (0.7 mL). To this deep orange coloured solution benzene (0.2 mL) was added. ^{1}H, ^{31}P, $^{31}P\{^{1}H\}$, ^{11}B and $^{11}B\{^{1}H\}$ NMR spectra were recorded after the given times/conditions.

Reaction with C_6D_6: In a nitrogen filled glovebox a screw cap NMR tube **4a** (5 mg, 11 μmol, 1 eq) was dissolved in C_6D_6 (0.7 mL). ^{1}H, ^{31}P, $^{31}P\{^{1}H\}$, ^{11}B and $^{11}B\{^{1}H\}$ NMR spectra were recorded after the given intervals of time.

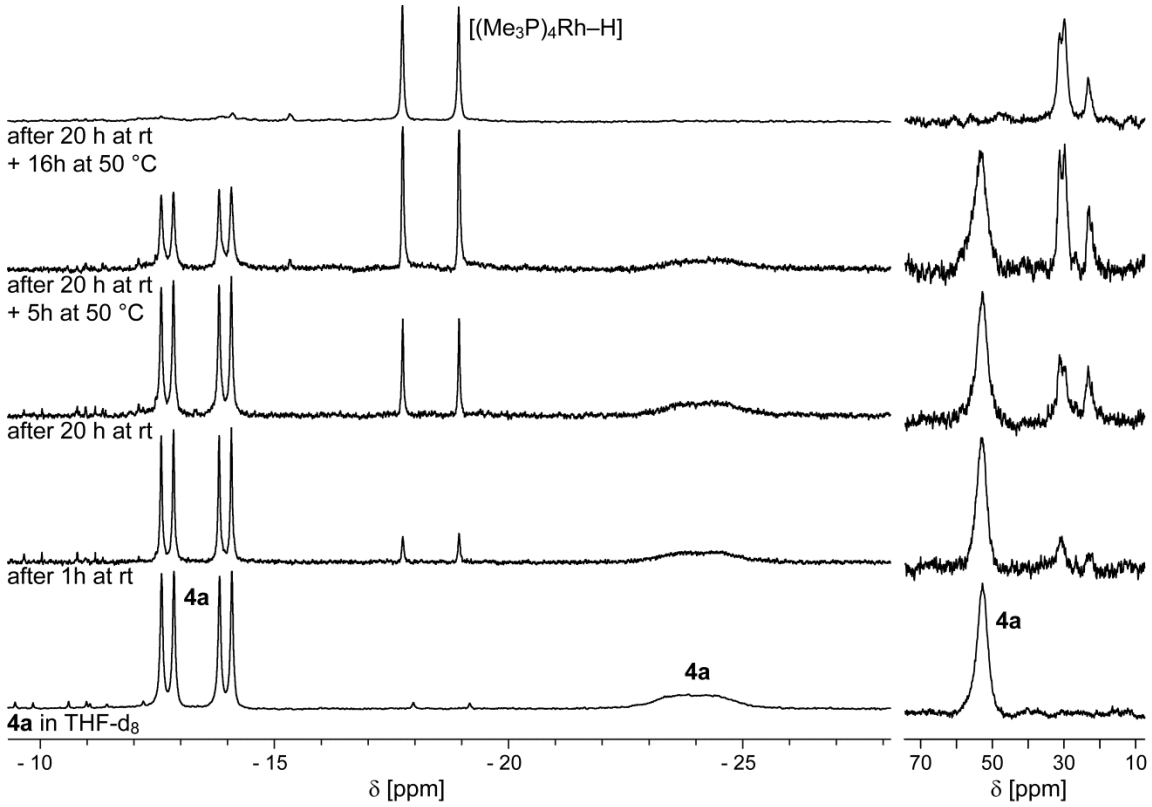

Figure S14. $^{31}P\{^{1}H\}$ (left) and $^{11}B\{^{1}H\}$ NMR spectra (right) of **4a** in THF-d_8/C_6H_6 after the given intervals of time (rt, 122 and 96 MHz, respectively).

Complex **4a** is clearly reacting with C_6H_6 (Figure S14), however, the rate is relatively small (ratio **4a**/[$(Me_3P)_4$Rh–H] (Figure S15). As product [$(Me_3P)_4$Rh–H] is identified by its characteristic $^{31}P\{^{1}H\}$ NMR signal (d, –18.4 ppm, $J_{P\text{-}Rh}$ = 146 Hz) in agreement with literature data.[S6] In addition small signals in the range of –8 to –15 ppm suggest the formation of additional unidentified species.

By $^{11}B\{^1H\}$ NMR spectroscopy three boron containing products are detected: dmabB–Ph (29.4 ppm), B_2dmab_2 (28.9 ppm) and a unidentified species with a signal at 23.9 ppm. The latter may be assigned to a species containing a N_2BO moiety possibly due to adventitious moisture.[S7]

This is also corroborated by GC/MS analysis of the mixture (not shown): signals are detected with m/z ratios and isotope patterns corresponding to dmabB–Ph and B_2dmab_2, respectively. In addition a small signal suggestive for $O(Bdmab)_2$ is observed.

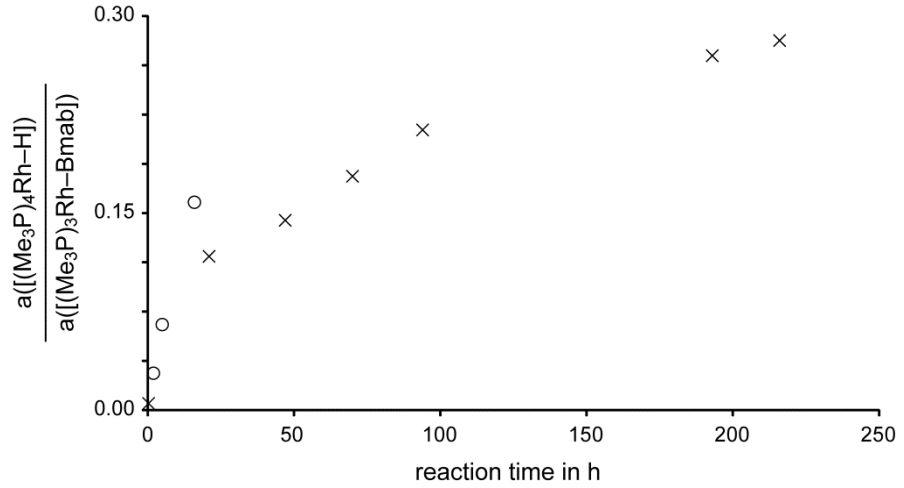

Figure S15. Area ratio a([$(Me_3P)_4$Rh–H]) / a([$(Me_3P)_3$Rh–Bdmab]) of the $^{31}P\{^1H\}$ NMR signals of the respective compounds during the reaction of **4a** with C_6H_6/C_6D_6 (○ in C_6H_6, × in C_6D_6).

Moreover, a sample of **4a** in C_6D_6 shows a comparable reaction to the respective deuterated products (Figure S15). Again, these findings are corroborated by GC/MS analysis of the mixture: two main signals are detected corresponding to B_2dmab_2 and dmabB–C_6D_5.

The reactivity of **4a** with aromatics and especially the puzzling formation of the tetrakis-trimethylphosphine complex [$(Me_3P)_4$Rh–H/D] from the tris-trimethylphosphine complex **4a** remains subject of further studies. Noteworthy, the (reductive) formation of the symmetrical diborane(4) B_2dmab_2 may imply the formation of (paramagnetic) Rh species in low oxidation states or Rh metal that are not necessarily detected by NMR spectroscopy by the means described.

However, it can be stated that the C–H/D bond activation of C_6D_6/C_6H_6 by **4a** is slow and in particular that NMR measurements may be conducted in C_6D_6 within a period

of ca. 10 h at rt without being compromised by extensive decomposition. Note also that this is in line with the reported C–H activation of aromatics by the related complex [$(Et_3P)_3Rh$–Bpin].[S8]

2. Computational Details

All quantum chemical calculations have been performed with the Gaussian 09 set of programs.[S9a] The B3LYP hybrid functional was employed for all calculations.[S9b,c] All atoms except rhodium were described by a standard triple zeta all-electron basis set augmented with one set of polarisation functions (6-311G(d,p)). For rhodium, a double-zeta basis set optimised for the use with effective core potentials (ECP) in combination with the corresponding Stuttgart ECP was used.[S9d] Were possible, all geometry optimisations started from structures obtained from X-ray diffraction, or from slightly modified ones. All geometry optimisations were performed without any imposed symmetry constraints, and have been performed with the same combination of electronic structure method and basis set, as the subsequent frequency calculations. The relevant stationary points have been characterised as minima or transitions states by normal mode analysis based on analytical energy second derivatives. Standard convergence criteria as implemented in Gaussian 09 have always been met. Enthalpic and entropic contributions were calculated by means of statistical thermodynamics as implemented in the Gaussian 09 set of programs.

Table S3. Energies/enthalpies of the calculated stationary points.

Compound	$E_{el} + E_0$	$E_{el} + H_{298}^0$	$E_{el} + G_{298}^0$
PMe_3	-461.051524	-461.043825	-461.080914
$[(Me_3P)_3Rh–Bdmab]$ (**4a**)	-1939.068135	-1939.032827	-1939.132316
$[(Me_3P)_4Rh–Bdmab]$ (**5**)	-2400.109303	-2400.066339	-2400.180881
TS	-2400.106081	-2400.063005	-2400.179481

Table S4. Cartesian coordinates of the calculated stationary points.

PMe_3

P	0.00010	0.00000	-0.60210
C	-1.03820	1.27070	0.27950
H	-0.71810	2.27220	-0.01810
H	-2.08340	1.15650	-0.01780
H	-0.97030	1.18800	1.36900
C	1.61970	0.26370	0.27960
H	2.32650	-0.51470	-0.01760
H	2.04380	1.22560	-0.01820
H	1.51390	0.24680	1.36900
C	-0.58150	-1.53440	0.27950
H	-1.60880	-1.75780	-0.01840
H	0.04000	-2.38250	-0.01760
H	-0.54410	-1.43420	1.36900

$[(Me_3P)_3Rh–Bdmab]$ (4a)

C	-3.39180	0.02860	-0.72010
C	-4.58410	0.07630	-1.43350
H	-4.58640	0.08620	-2.51750
C	-5.78900	0.11240	-0.71910
H	-6.72750	0.14950	-1.26090
C	-1.73060	0.04120	-2.55720
H	-2.17010	-0.79550	-3.11470
H	-0.64510	-0.00750	-2.64920
H	-2.08450	0.97020	-3.02300
C	-0.24010	-3.06800	-1.47810
H	0.35070	-2.85120	-2.37020
H	-1.22130	-2.60880	-1.59480
H	-0.35690	-4.15130	-1.38060
C	-0.48270	-3.03420	1.35870
H	-0.58530	-4.11860	1.26000
H	-1.46680	-2.57050	1.31000
H	-0.04260	-2.80580	2.33130
C	1.99000	-3.58430	0.16080
H	2.58800	-3.37430	1.04980
H	2.63500	-3.52880	-0.71590
H	1.59330	-4.60060	0.23810
B	-1.16260	-0.04510	-0.00090
N	-2.06900	-0.01240	-1.15090
P	0.59860	-2.35260	0.01350
P	0.64930	2.25640	0.02480
Rh	0.93740	-0.04890	-0.00810
C	-3.39820	0.01890	0.69690
C	-4.59740	0.05640	1.39950
H	-4.61000	0.05050	2.48340
C	-5.79540	0.10250	0.67430
H	-6.73900	0.13190	1.20780
C	-1.75610	0.01700	2.54870
H	-2.13480	0.93320	3.02080
H	-0.67060	-0.00770	2.65080
H	-2.18180	-0.83470	3.09400
N	-2.08040	-0.02820	1.13970
C	-1.00030	3.02420	0.38770
H	-0.93170	4.11470	0.33450
H	-1.33510	2.73560	1.38420

H	-1.74440	2.67430	-0.32810
C	1.65340	3.23690	1.24880
H	2.72020	3.05140	1.12680
H	1.37160	2.92640	2.25710
H	1.46720	4.30980	1.14500
C	1.01960	3.15080	-1.56280
H	0.91880	4.23340	-1.43970
H	0.31240	2.81550	-2.32390
H	2.02440	2.92090	-1.91420
C	4.15250	0.18050	1.64770
H	3.86970	-0.68560	2.24960
H	3.78490	1.07130	2.15910
H	5.24370	0.22990	1.58030
C	4.21260	1.43410	-0.91830
H	5.29630	1.37950	-0.78150
H	3.86720	2.40570	-0.56700
H	3.99050	1.36080	-1.98540
C	4.40320	-1.32980	-0.73380
H	4.06600	-1.57080	-1.74410
H	4.32280	-2.22560	-0.12080
H	5.45420	-1.03000	-0.77520
P	3.35470	0.03920	-0.02700

[($Me_3P)_4$Rh–Bdmab] (5)

C	2.65500	-1.73330	-2.78550
H	3.32690	-2.56430	-3.02220
H	3.13770	-0.80340	-3.08880
H	1.73970	-1.85120	-3.36750
C	1.80480	-3.49650	-0.79740
H	0.82630	-3.67490	-1.24580
H	1.75150	-3.78440	0.25330
H	2.54230	-4.13660	-1.29240
C	4.02460	-1.83240	-0.35080
H	4.04050	-1.87250	0.73980
H	4.58260	-0.94840	-0.66340
H	4.52580	-2.72160	-0.74790
C	1.74190	1.97710	-2.85540
H	2.44500	1.20330	-3.16250
H	2.26950	2.67740	-2.20760
H	1.39910	2.51440	-3.74430
C	-0.53220	0.38480	-3.37850
H	-1.52500	0.05940	-3.07060
H	0.03430	-0.48840	-3.70150
H	-0.62830	1.07560	-4.22130
C	-0.78260	2.72030	-1.84780
H	-0.82690	3.22680	-2.81630
H	-0.40180	3.41540	-1.10000
H	-1.78840	2.42140	-1.55370
C	1.74200	-1.97710	2.85530
H	1.39930	-2.51440	3.74430
H	2.44520	-1.20330	3.16240
H	2.26960	-2.67750	2.20750
C	-0.53200	-0.38480	3.37850
H	-1.52490	-0.05940	3.07070
H	0.03450	0.48840	3.70160
H	-0.62810	-1.07560	4.22130
C	-0.78250	-2.72030	1.84790
H	-0.82670	-3.22680	2.81640

H	-0.40170	-3.41540	1.10010
H	-1.78830	-2.42140	1.55380
C	2.65490	1.73340	2.78550
H	3.13760	0.80350	3.08880
H	1.73960	1.85140	3.36740
H	3.32680	2.56440	3.02220
C	1.80480	3.49650	0.79720
H	0.82620	3.67500	1.24570
H	1.75150	3.78440	-0.25350
H	2.54220	4.13660	1.29230
C	4.02450	1.83240	0.35080
H	4.52580	2.72170	0.74790
H	4.04050	1.87250	-0.73970
H	4.58250	0.94840	0.66350
P	2.26060	-1.68990	-0.96010
P	0.30440	1.21520	-1.94350
P	0.30450	-1.21530	1.94350
P	2.26060	1.69000	0.96010
Rh	0.74860	-0.00000	-0.00000
B	-1.38400	-0.00000	0.00000
N	-2.31100	-0.94910	-0.63910
N	-2.31100	0.94910	0.63920
C	-3.63090	-0.58770	-0.39340
C	-2.01360	-2.13850	-1.40570
C	-3.63090	0.58760	0.39350
C	-2.01360	2.13850	1.40570
C	-4.82790	-1.17850	-0.78530
H	-2.39740	-3.04220	-0.91560
H	-0.93250	-2.21990	-1.49830
H	-2.45360	-2.09340	-2.40970
C	-4.82790	1.17850	0.78530
H	-2.39740	3.04220	0.91560
H	-0.93260	2.21990	1.49830
H	-2.45370	2.09340	2.40970
H	-4.83590	-2.08040	-1.38650
C	-6.02960	-0.58030	-0.38600
H	-4.83600	2.08030	1.38650
C	-6.02960	0.58020	0.38600
H	-6.97120	-1.02810	-0.68370
H	-6.97120	1.02800	0.68370

TS

C	3.94140	-1.23680	1.59380
H	4.76120	-1.95930	1.53660
H	3.45280	-1.34780	2.56260
H	4.35620	-0.22910	1.53400
C	3.94530	-1.64930	-1.17440
H	4.35960	-0.66460	-1.40140
H	3.46310	-2.02930	-2.07610
H	4.76570	-2.32350	-0.91010
C	2.40170	-3.32160	0.50450
H	1.81670	-3.73390	-0.31760
H	1.81910	-3.44900	1.41790
H	3.33830	-3.88150	0.59480
C	3.82950	2.48070	0.05280
H	4.35050	1.72210	-0.53530
H	3.97570	2.24710	1.10960
H	4.27960	3.45690	-0.15510

C	2.10110	3.22580	-2.04680
H	1.09390	3.39000	-2.43710
H	2.62100	2.55280	-2.73090
H	2.63070	4.18390	-2.02840
C	1.50080	3.97230	0.60360
H	2.13450	4.83260	0.36520
H	1.56710	3.78000	1.67620
H	0.46390	4.22680	0.37610
C	0.30180	-2.63950	-2.65480
H	0.04950	-2.78990	-3.70890
H	-0.41520	-3.18150	-2.03680
H	1.29340	-3.05590	-2.47270
C	-1.33890	-0.39500	-3.06040
H	-1.50220	0.68210	-3.01070
H	-2.17800	-0.88230	-2.56370
H	-1.30960	-0.70590	-4.10900
C	1.40870	-0.16280	-3.51260
H	1.21340	-0.62150	-4.48660
H	2.44930	-0.33490	-3.23980
H	1.25250	0.91320	-3.59810
C	0.26940	-1.56200	3.35070
H	1.22590	-2.08150	3.27780
H	-0.50820	-2.23030	2.97950
H	0.07300	-1.33470	4.40290
C	-1.24090	0.79370	2.97630
H	-2.11960	0.21820	2.68480
H	-1.34210	1.79360	2.55150
H	-1.20220	0.86740	4.06710
C	1.53310	0.97900	3.30680
H	1.31350	0.92880	4.37750
H	1.48210	2.02210	2.99250
H	2.54740	0.62120	3.13470
P	2.70730	-1.50730	0.21790
P	2.00750	2.44670	-0.35200
P	0.25410	-0.83220	-2.21030
P	0.29830	-0.01220	2.32100
Rh	0.63040	-0.27080	0.02140
B	-1.45520	-0.04320	0.00130
N	-2.30810	1.12560	-0.23780
N	-2.44110	-1.10760	0.24130
C	-3.65060	0.77990	-0.13970
C	-1.91340	2.47350	-0.56700
C	-3.73340	-0.60290	0.15560
C	-2.20490	-2.50860	0.51170
C	-4.80380	1.54350	-0.28350
H	-2.35080	2.80280	-1.51880
H	-0.82850	2.49140	-0.65240
H	-2.22110	3.19280	0.20400
C	-4.96960	-1.22210	0.30560
H	-2.62890	-2.81400	1.47760
H	-1.12600	-2.66570	0.52760
H	-2.65030	-3.15100	-0.25960
H	-4.74870	2.60250	-0.50850
C	-6.04610	0.91360	-0.13080
H	-5.04050	-2.28000	0.53100
C	-6.12770	-0.44700	0.15890
H	-6.95450	1.49570	-0.23990
H	-7.09910	-0.91530	0.27320

3. Crystallographic Data

Unless noted otherwise crystals were transferred into inert perfluoroether oil inside a nitrogen filled glovebox and, outside of the glovebox, mounted on top of a human hair and transferred into the cold nitrogen gas stream on the diffractometer.[S10a] The data were collected on an Oxford Diffraction Xcalibur E instrument using monochromated MoKα radiation. The data were processed, including an empirical absorption correction, employing the CrysAlisPro software.[S10b] All structures were solved employing SIR-92 and refined anisotropically for all non-hydrogen atoms by full-matrix least squares on all F^2 using SHELXL-2013 or -2014/7.[S10c,d] Hydrogen atoms were refined employing a riding model. During refinement and analysis of the crystallographic data the programs WinGX, PLATON, SQUEEZE, Mercury and Diamond were used.[S10e-i]

[$(Me_3P)_4$Rh–Bpin] (3): The crystal is non-merohedrally twinned by 180° rotation about the reciprocal [0 1 0] axis. The two components were indexed separately and integrated taking both components into account (HKLF5-file). The refinement was performed against the data of both components. The structure solution was performed on a dataset containing only the data of the main component (R_{int} = 0.0801). The twin factor refined to 0.4123(7). Refinement in alternative, e. g. monoclinic cell settings was attempted but leads to heavy disorder and was abandoned.

[$(Me_3P)_3$Rh–Bdmab] (4a): The ASU contains half a molecule of [$(Me_3P)_3$Rh–Bdmab] situated on a two-fold axis causing disorder of the *trans*-B PMe_3 moiety. During the refinement similarity restraints (SADI) on P–C distances and C–P–C angles were employed.

$(Me_3P)_3$Rh–Bdbab (4b): The unit cell contains besides two equivalent molecule of **4b** one molecule of *n*-pentane and two equivalent molecules of toluene.

1) The *n*-pentane molecule is disordered on an inversion centre; all C–C distances were restraint to 1.54 Ang (DFIX). The SOF refined to ca. 1/2 and was eventually fixed to 1/2.

2) The disordered PhMe molecule was refined employing geometrical restraints:

- the phenyl moiety was refined as regular hexagon (AFIX 66)
- the H_3C–C(ipso) distance was restraint to 1.54 Ang (DFIX)
- the two H_3C–C(ortho) distance were restraint to equivalence (SADI)
- all ADP were restraint to approximate isotropic behaviour (ISOR)

[$(Me_3P)_4$Rh–Bdmab] (5): Crystallisation was conducted as *in situ* crystallisation from a saturated solution of [$(Me_3P)_3$Rh-Bdmab] **4a** in PMe_3. In a thin-walled glass tube of 0.5 mm outer diameter the yellow solution (approx. 0.2 μl, 1.5 mm height) was placed and the capillary was flame-sealed. In this capillary microcrystals had formed, presumably due to evaporation of PMe_3 during the preparation procedure. After several attempts to obtain single crystals by repeated careful warming (with the finger tips and/or warm water) and cooling (ice/water, evaporation of acetone) two well-developed individual rhombohedral crystals were obtained (ca. 0.1×0.1×0.1 mm^3). At this point it was decided to proceed with these two crystals together, as attempts to separate them by careful shaking were unsuccessful and to dissolve and recrystallise was not very promising. The capillary was immersed in the nitrogen gas stream on the diffractometer and cooled to –40 °C within 30 min and after 15 min at this temperature to –80 °C within 30 min. At this point the two crystals had grown to two adjacent individual rhombohedral crystals of ca. 0.18×0.20×0.24 mm^3 and 0.09×0.10×0.11 mm^3 size, whilst the solution had completely discoloured. In order to fix the crystals inside the capillary the temperature was lowered to –98 °C (175 K), below the melting point of PMe_3 that solidified to a polycrystalline material that embedded the crystals. In this form the larger of the two crystals was centred in the beam and cell determination and data collection was performed.

The diffraction pattern showed at higher diffraction angles ($d \leq 1.5$) well resolved reflections that were indexed using two orientation matrices, in accordance with the two crystals observed optically. At these higher diffraction angles only a negligible number of overlapping reflections were observed and the orientation matrices were used for integration. However, at lower diffraction angles ($d \geq 1.5$) a considerable number of reflections showing characteristics of powder pattern were observed originating presumably from polycrystalline PMe_3. The diffraction data for both

crystals were separately integrated to give two datasets. For solution and refinement of the structure only the dataset with the better I/σ(I) ratio was used. Presumably as a consequence of the presence of polycrystalline PMe_3 or the second crystal 7 low angle reflections of high Fo/Fc were observed that were omitted from the refinement.

Table S2. Selected crystallographic data collection parameters; see above for further details.

	3	**4a**	**4b**	**5**	$[(Me_3P)_2Rh CH_2PMe_2]_2$
Chemical formula	$C_{18}H_{48}BO_2P_4Rh$	$C_{17}H_{37}BN_2P_3Rh$	$C_{29}H_{45}BN_2P_3Rh \cdot C_7H_8 \cdot ½\ C_5H_{12}$	$C_{20}H_{46}BN_2P_4Rh$	$(C_9H_{26}P_3Rh)_2$
Mass (g mol^{-1})	534.16	476.11	756.50	552.19	660.23
Cryst. dim. (mm^3)	0.16 x 0.18 x 0.50	0.18 x 0.36 x 0.42	0.27 x 0.28 x 0.47	0.24 x 0.20 x 0.18[a]	0.27 x 0.28 x 0.30
Crystal system	triclinic	monoclinic	triclinic	monoclinic	monoclinic
Space group (no.)	$P\bar{1}$ (2)	$P2/n$ (13)	$P\bar{1}$ (2)	$P2_1/c$ (14)	$P2_1/n$ (14)
Z	2	2	2	4	2
a (Å)	9.2105(6)	6.6650(1)	9.9185(1)	9.2189(4)	9.6621(2)
b (Å)	12.290(1)	13.9554(2)	11.7946(2)	19.0437(7)	12.0824(2)
c (Å)	12.381(1)	12.2545(2)	18.9805(2)	15.9428(6)	13.1972(2)
α (°)	90.471(8)	90	72.324(1)	90	90
β (°)	98.184(6)	91.403(1)	80.778(1)	94.531(4)	108.536(2)
γ (°)	90.520(8)	90	67.981(1)	90	90
Volume (Å^3)	1387.1(2)	1139.48(3)	1957.87(5)	2790.2(2)	1460.74(5)
D_{calcd} (Mg m^{-3})	1.279	1.388	1.283	1.314	1.501
T (K)	100(2)	102(2)	100(2)	175(2)	100(2)
Radiation, λ (Å)	MoKα, 0.71073	MoKα, 0.71073	MoKα, 0.71073	MoKα, 0.71073	MoKα, 0.71073
μ (mm^{-1})	0.856	0.963	0.587	0.851	1.462
Refl. coll. / unique	25564 / 25564[a]	105629 / 3327	249085 / 11747	201179 / 8105	46335 / 3890
No. of param. / restr.	252 / 0	131 / 6	482 / 92	267 / 0	126 / 0
θ range (°)	2.23 – 30.00	2.21 – 30.00	2.22 – 30.86	2.14 – 30.00	2.30 – 29.00
R_{int}	0.0801[a]	0.0434	0.0454	0.0879	0.0277
GooF on F^2	1.006	1.092	1.129	1.141	1.069
R_1 [$I > 2\sigma(I)$]	0.0380	0.0277	0.0423	0.0415	0.0200
wR_2 (all data)	0.0911	0.0729	0.1040	0.0876	0.0473
Peak / hole (e·Å^{-3})	1.539 / –2.467	1.322 / –1.120	1.430 / –0.695	0.618 / –0.697	2.283 / –0.604
CCDC no.	1037664	1037663	1037665	1037666	1037662

For further crystallographic details refer to the crystallographic data available as supporting information or from the Cambridge Crystallographic Centre (CCDC Nos. 1037662 – 1037666).

4. References

S1 C. Borner and C. Kleeberg, *Eur. J. Inorg. Chem.,* 2014*,* 2486–2489.

S2 R. T. Price, R. A. Andersen and E. L. Muetterties, *J. Organomet. Chem*, 1989, **376**, 407–417.

S3 G. R. Fulmer, A. J. M. Miller, N. H. Sherden, H. E. Gottlieb, A. Nudelman, B. M. Stoltz, J. E. Bercaw and K. I. Goldberg, *Organometallics,* 2010, **29**, 2176–2179.

S4 V. V. Mainz and R. A. Andersen, *Organometallics*, 1984, **3**, 675–678.

S5 (a) C. Dai, G. Stringer, T. B. Marder, A. J. Scott, W. Clegg and N. C. Norman, *Inorg. Chem.*, 1997, **36**, 272–273. (b) J. Zhu, Z. Lin and T. B. Marder, *Inorg. Chem.,* 2005, **44**, 9384–9390; (c) H. Braunschweig, P. Brenner, A. Müller, K. Radacki, D. Rais and K. Uttinger, *Chem.–Eur. J.,* 2007, **13**, 7171–7176.

S6 (a) D. Zargarian, P. Chow, N. J. Taylor and T. B. Marder, *J. Chem. Soc., Chem. Commun.*, 1989, 540–544; (b) M. Paneque and P. M. Maitlis, *J. Chem. Soc., Chem. Commun.*, 1989, 105–106.

S7 (a) R. Goetze, H. Nöth, H. Pommerening, D. Sedlak and B. Wrackmeyer, *Chem. Ber.*, 1981, **114**, 1884–1893; (b) X. Xie, M. F. Haddow, S. M. Mansell, N. C. Norman and C. A. Russell, *Dalton Trans.*, 2012, **41**, 2140–2147; (c) H. Nöth and B. Wrackmeyer, *Chem. Ber.*, 1973, **106**, 1145–1164; (d) L. Weber, I. Domke, W. Greschner, K. Miqueu, A. Chrostowska and P. Baylère, *Organometallics*, 2005, **24**, 5455–5463; (e) C. Kleeberg, J. Grunenberg and X. Xie, *Inorg. Chem.*, 2014, **53**, 4400−4410.

S8 (a) M. Teltewskoi, J. A. Panetier, S. A. Macgregor and T. Braun, *Angew. Chem. Int. Ed.*, 2010, **49**, 3947–3951; (b) S. I. Kalläne and T. Braun, *Angew. Chem. Int. Ed.*, 2014, **53**, 9311–9315; (c) S. I. Kalläne, M. Teltewskoi, T. Braun and B. Braun, *Organometallics*, 2015, DOI: 10.1021/om500952x.

S9 (a) Gaussian 09, Revision **D.01**, M. J. Frisch, G. W. Trucks, H. B. Schlegel, G. E. Scuseria, M. A. Robb, J. R. Cheeseman, G. Scalmani, V. Barone, B. Mennucci, G. A. Petersson, H. Nakatsuji, M. Caricato, X. Li, H. P. Hratchian, A. F. Izmaylov, J. Bloino, G. Zheng, J. L. Sonnenberg, M. Hada, M. Ehara, K. Toyota, R. Fukuda, J. Hasegawa, M. Ishida, T. Nakajima, Y. Honda, O. Kitao, H. Nakai, T. Vreven, J. A. Montgomery, Jr., J. E. Peralta, F. Ogliaro, M. Bearpark, J. J. Heyd, E. Brothers, K. N. Kudin, V. N. Staroverov, R. Kobayashi, J. Normand, K. Raghavachari, A. Rendell, J. C. Burant, S. S. Iyengar, J. Tomasi, M. Cossi, N. Rega, J. M. Millam, M. Klene, J. E. Knox, J. B. Cross, V. Bakken, C. Adamo, J. Jaramillo, R. Gomperts, R. E. Stratmann, O. Yazyev, A. J. Austin, R. Cammi, C. Pomelli, J. W. Ochterski, R. L. Martin, K. Morokuma, V. G. Zakrzewski, G. A. Voth, P. Salvador, J. J. Dannenberg, S. Dapprich, A. D. Daniels, Ö. Farkas, J. B. Foresman, J. V. Ortiz, J. Cioslowski and D. J. Fox, Gaussian, Inc., Wallingford CT, 2009; (b) A. D. Becke, *Phys. Rev. B*, 1988, **38**, 3098 – 3100; (c) C. Lee, W. Yang and R. G. Parr, *Phys. Rev. B*, 1988, **37**, 785 – 789; (d) D. Andrae, U. Häußermann, M. Dolg, H. Stoll and H. Preuß, *Theor. Chim. Acta*, 1990, **77**, 123 – 141.

S10 (a) D. Stalke, *Chem. Soc. Rev.,* 1998, **27**, 171–178; (b) CrysAlisPro, Agilent Technologies, Versions 1.171.36.24a–1.171.37.35, 2012–2014; (c) A. Altomare, G. Cascarano, C. Giacovazzo and A. Guagliardi, *J. Appl. Crystallogr.,* 1993, **26**, 343–350; (d) G. M. Sheldrick, *Acta Cryst.,* 2008, **A64**, 112–122; e) L. J. Farrugia, *J. Appl. Crystallogr.,* 1999, **32**, 837–838; (f) C. F. Macrae, I. J. Bruno, J. A. Chisholm, P. R. Edgington, P. McCabe, E. Pidcock, L. Rodriguez-Monge, R. Taylor, J. van de Streek and P. A. Wood, *J. Appl. Cryst.,* 2008, **41**, 466–470; (g) A. L. Spek, PLATON - A Multipurpose Crystallographic Tool, Utrecht University, Utrecht, The Netherlands, 1998; (h) K. Brandenburg, Crystal Impact GbR, Diamond 3.2k, Bonn, Germany, 2014; (i) P. v. d. Sluis and A. L. Spek, *Acta Crystallogr.,* 1990, **A46**, 194–201.